2023-10-04

Dynamical oceanographic processes impact on reef manta ray behaviour: Extreme Indian Ocean Dipole influence on local internal wave dynamics at a remote tropical atoll

Robinson, E

10.1016/j.pocean.2023.103129
Progress in Oceanography
Elsevier

Dynamical oceanographic processes impact on reef manta ray behaviour: Extreme Indian Ocean Dipole influence on local internal wave dynamics at a remote tropical atoll.

Edward Robinson[1], Phil Hosegood[1], Adam Bolton[1]

[1] University of Plymouth, Drakes Circus, Plymouth, PL4 8AA, United Kingdom.

Corresponding author: Edward Robinson, edward.robinson@plymouth.ac.uk, +44(0)7483819965

Co-author contacts: phil.hosegood@plymouth.ac.uk (Phil Hosegood), adam.bolton@plymouth.ac.uk (Adam Bolton)

Author contributions:

Edward Robinson: Conceptualization; Methodology; Data Curation; Formal Analysis; Investigation; Data Curation; Writing – Draft, Review, Editing; Visualisation.

Phil Hosegood: Conceptualization; Methodology; Investigation; Resources; Data Curation; Writing – Draft, Review, Editing; Supervision; Project Administration; Funding acquisition

Adam Bolton: Investigation; Resources; Data Curation; Visualization

Funding sources: Funding for this work was provided by the Garfield Weston Foundation, and Bertarelli Foundation.

Keywords: Internal Waves; Physical Oceanography; Biodiversity; Local Movements; Indian Ocean Dipole; Chagos Archipelago.

Abstract

Physical oceanographic observations were made with subsurface, taut-line moorings at Egmont Island, a tropical atoll within the Chagos Archipelago in the central Indian Ocean, to elucidate the dynamics of near-bed cold-water intrusions implicated in driving local aggregations of reef manta rays (*M. Alfredi*). Manta have been previously shown to aggregate within 'Manta Alley', a lipped gully at 65 m depth along the north coast, at times when the surface to bottom temperature difference was highest. We here identify the dynamical processes driving these temperature differences and shaping the foraging landscape at Egmont, and equivalent small-scale atolls, improving our understanding of manta behavior at hotspots where they are most vulnerable to exploitation.

The thermal regime within Manta Alley is shown to be governed at several spatiotemporal scales. The extreme 2019 Indian Ocean Dipole event drove a depression of the 26 °C isotherm to a depth of 115 m precluding the observation of cooling within the alley. As the thermocline shoaled with the change in phase of the IOD, near bed cold water flushing was seen with tidal periodicity within the gully. The internal tide is accompanied by high frequency internal waves with periods of *O*(5 minutes) which are shown to promote mixing through shear instability, evidenced by subcritical Richardson numbers, with surface-seabed temperature differences ~ 4 °C observed throughout a tidal period.

Our results highlight a level of heterogeneity in oceanographic dynamics at sub-atoll spatial scales within an environment in which these processes are rarely resolved. Whilst the physical mechanisms through which these dynamics drive foraging within the resident manta population remain unclear, the generation of turbulence by high frequency internal wave events as shown here may influence zooplankton distributions, improving feeding efficiency at discrete locations within atolls. Our results thus highlight the need to account for fine scale changes in oceanographic conditions when attempting to explain habitat utilization by mobile species.

1 - Introduction

Within tropical regions, manta rays are a highly visible, but threatened species for which various protection measures have been implemented regionally. Such measures rarely, if ever, account for the physical drivers that govern their distribution and behaviour; as oceanographic conditions change, manta move into different biophysical habitats at both inter, and sub-atoll scales, raising the likelihood that current location specific protection measures are deficient. At regional scales, manta ray populations have been observed to track elevated levels of primary productivity (Jaine *et al.*, 2014; Weeks *et al.*, 2015; Armstrong *et al.*, 2016, 2019) and coastal populations have been observed to respond to changes in food availability and physical properties of the water column, including temperature, tidal timing, and local current regime (e.g. Rohner *et al.*, 2013; Armstrong *et al.*, 2021).

Recent studies have shown that manta exhibit strong site fidelity at local (i.e. single island) scales (Peel *et al.*, 2019; Andrzejaczek *et al.*, 2020) but with variability at sub-tidal timescales (Harris *et al.*, 2021). The mid-ocean atolls inhabited by these populations are characterised by steep slopes (Velmurugan, 2015), and are known to promote energetic internal processes, such as internal waves and elevated mixing though turbulent dissipation (Wolanski and Delesalle, 1995; Fu *et al.*, 2016; Rayson *et al.*, 2018). Internal waves are capable of advecting cold water upslope over large horizontal and vertical distances (Klymak *et al.*, 2012; Hosegood *et al.*, 2019; Reid *et al.*, 2019), thereby impacting nutrient supply into the photic zone. These dynamics are driven by a range of forcing processes, generally tidal and, in some limited capacity, through wind and atmospheric forcing (Farmer and Armi, 1999; Holloway and Merrifield, 1999; Balmforth and Peacock, 2009; Nikurashin and Ferrari, 2010). The timescale for bottom-up support via nutrient injection is on the order of days, and so the fine scale dynamical variability at these oceanic island habitats, and the comparatively short temporal scales over which a community response is observed (Harris et al., 2021), implies that localised processes generate sites of improved foraging efficiency of zooplankton which the manta exploit at discrete times.

Whilst suggestions have been made as to which processes drive aggregation events, there have been limited physical in-situ observations to provide insight into the oceanographic regime over fine scales, with observations typically limited to single point temperature and tidal timings (Armstrong *et al.*, 2016; Peel *et al.*, 2019). Prior research efforts have also typically taken a relatively isolated approach to understanding the influence of physical dynamics on the ecosystem, often focusing on a single physical parameter (e.g. tide) without further insight into the resultant fine scale dynamical variability (e.g. Armstrong *et al.*, 2021). This approach results in the inability to identify fine-scale dynamical processes that may act as drivers for manta behaviour, hindering the development of adequate conservation strategies that are typically derived from coarse scale models and remote observations that are unable to account for sub grid scale dynamics occurring locally within atolls. Improving our ability to understand fine scale dynamics will enable the focusing of protection efforts on specific locations which are disproportionately important to host species in terms of residence time and abundance, allowing for more efficient use of monitoring and enforcement resources.

In this paper we identify localised hydrodynamics responsible for the differences between the surface and near bed temperatures that have been identified as a dominant indicator of manta aggregation at an atoll in the tropical Indian Ocean (Harris et al., 2021) using moored, high resolution, in-situ observations. Egmont Atoll is a steep sloped atoll within the Chagos Archipelago located within the central Indian Ocean and is the site of the world's second largest no-take Marine Protected Area (Fig. 1). Long term remotely sensed observations of chlorophyll-a (Chl-a) highlight a sustained increase in local primary production throughout the archipelago (Fig. 1a). However, the complete picture of primary production is obscured by the concentration of phytoplankton within the deep chlorophyll maximum (DCM) at a typical depth of >50 m corresponding to the base of the surface mixed layer, rendering it usually invisible to satellite-based sensors. Here we demonstrate that physical processes at a wide range of spatiotemporal scales act to govern the biophysical regime at Egmont atoll and are responsible for generating the site preferentiality for resident manta rays shown in Harris et al. (2021)

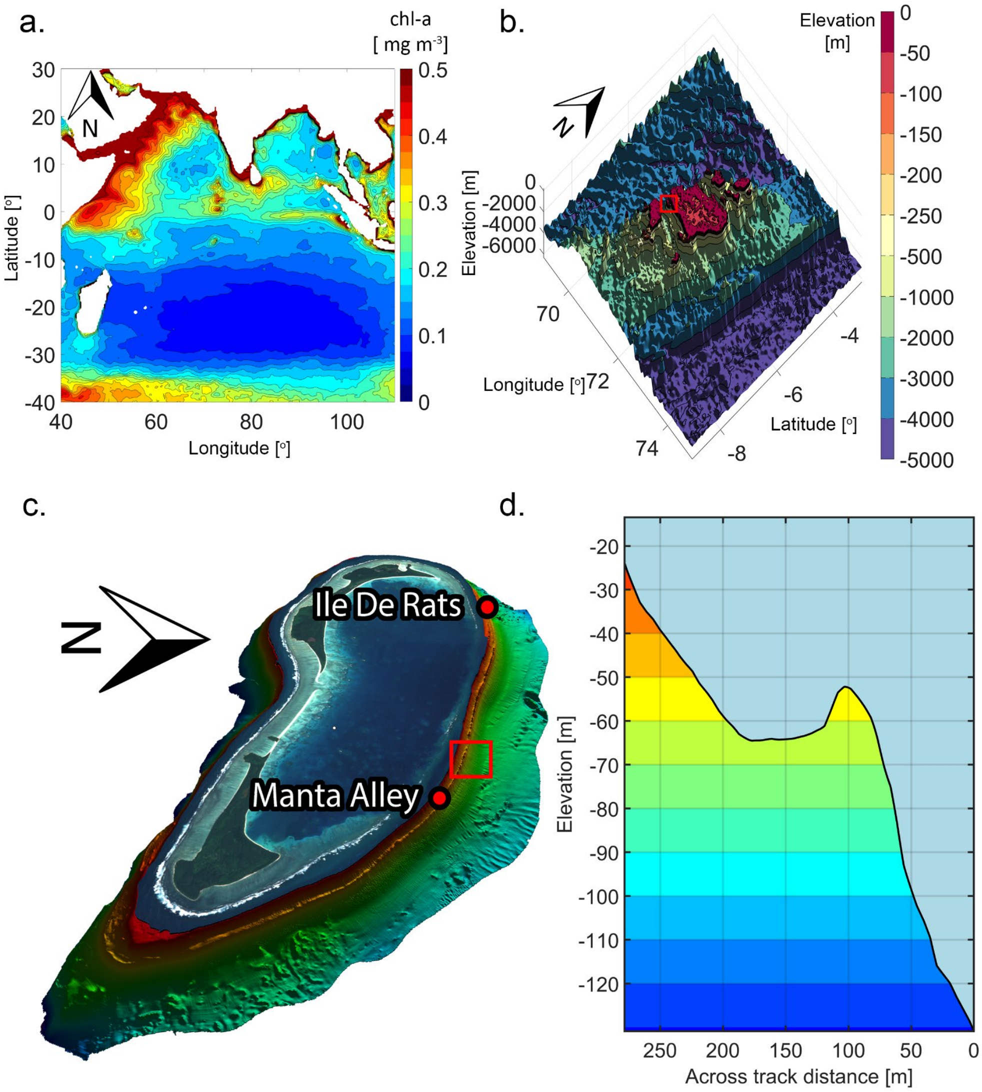

Fig. 1. a) January 2019 – January 2021 Chl-a mean in the Indian Ocean with the location of the Chagos Archipelago highlighted. Data from CMEMS Biogeochemical hindcast (10.48670/moi-00019) at monthly timesteps. b) GEBCO bathymetry of the wider archipelago with the location of Egmont Atoll annotated c) High resolution multibeam bathymetry of Egmont atoll showing the steep slopes which are greatly underrepresented within the GEBO bathymetry, and d) a representative cross-section of Manta Alley. Inset Landsat image courtesy of the U.S. Geological Survey. GEBCO 2023 Grid (doi:10.5285/f98b053b-0cbc-6c23-e053-6c86abc0af7b) courtesy of GEBCO Compilation Group (2023)

Here we show that the cold water, near-bed intrusions at Egmont are localised and intermittent, occurring predominantly at tidal periods but with higher frequency waves accompanying the tidal carrier wave as observed elsewhere (e.g. Hosegood and Van Haren, 2004). We further observe significant variability in internal wave behaviour and characteristics at different sites separated by short horizontal distances. Finally, we demonstrate that the depth to which cooling extends is dictated by the prevailing regional conditions where the IOD is responsible for migration of the thermocline at interseasonal time scales.

This paper is structured as follows; firstly the methodology is presented, including moored in-situ observations, and supporting remotely sensed data and numerical model output. We then briefly explore the characteristics of the dynamical mechanisms that are implicated in driving the temperature differences at both local and basin scales. Results are then presented, beginning with the basin-scale evolution of stratification in response to the extreme 2019 IOD event which coincided with the first research cruise, followed by characterisation of the background tidal environment, and its evolution over the course of the observation period. The impact of the stratification, specifically the evolution of thermocline depth, is considered in relation to local thermal variability at tidal and higher frequencies, as well as the role of high-frequency internal waves in promoting overturning and mixing. The implications of the dynamics in driving the local thermal changes are then discussed, with emphasis on the biophysical impacts likely to be responsible for the aggregations seen in Harris et al. (2021) and their applicability to alternative sites of similar scale which may also be oversimplified by use of remote observations and coarse-scale numerical model output.

2 - Methodology

2.1 - Study region and cruise timings

Data were obtained from two research cruises to the Chagos Archipelago conducted during the transition period between the south-east and north-west monsoon. The first cruise spanned the period 13/11/2019 – 03/12/2019 (hereafter referred to as 'November') and the second, approximately 4 months later, the period 07/03/2020 – 18/03/2020 (hereafter referred to as 'March'). Whilst both cruises fell between the monsoon seasons when winds were expected to be light, the prevailing meteorological conditions nonetheless varied; wind direction during November was north-easterly (rather than the expected south-easterly) and predominantly north-westerly during March; below we identify the role played by the especially strong IOD influence during November in generating the unusual wind direction. Air temperature in November averaged 28.5 °C, whilst March was warmer on average at 29 °C.

The specific geographic focus of this paper is constrained to Egmont (Fig. 2), an atoll on the southwestern flank of the archipelago, approximately 9 km south of Great Chagos Bank (GCB). The channel between Egmont and Great Chagos Bank on the north-eastern flank of Egmont is 200-300 m deep, with the drop-off to the south being considerably deeper, extending to over 1000 m depth. The steep slopes, which routinely exceed 30° at depths <150 m, surrounding Egmont (Fig. 2b) are characteristic of similar volcanic islands (Velmurugan, 2015) and present a challenge to the deployment of subsurface moorings that may slip down the slope. Additionally, vessel-based acoustic Doppler current meter (ADCP) measurements are challenging due to the obstruction of one or more beams by the seabed when sampling close to the atoll flanks.

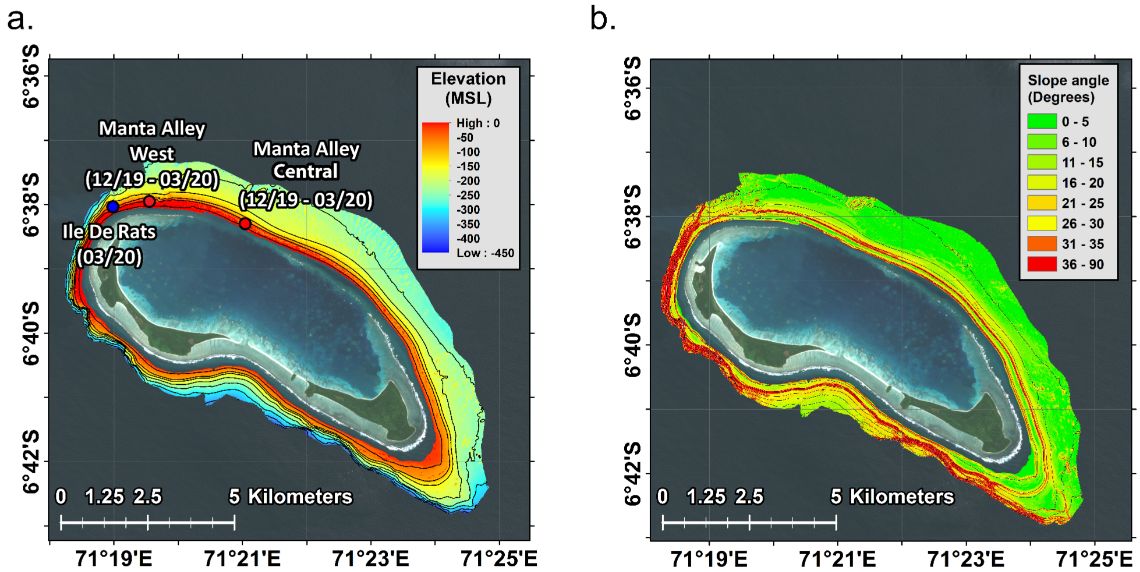

Fig. 2. a) Top-down view of Egmont with bathymetry overlaid on Landsat true colour imagery, indicated are the locations of mooring deployments with long-term moorings marked in red, and short-term moorings marked in blue. b) Local slope map of Egmont atoll calculated at 1 m cell size from multibeam bathymetry. Note the steep slopes which fringe the atoll and the comparatively flat slope within the gully of Manta Alley on the northeast flank. Landsat imagery courtesy of the U.S. Geological Survey.

The atoll is elliptical and approximately 11.0 km along the major axis and 4.3 km along the minor, with the major axis-oriented west-northwest to east-southeast. Most of the internal area of the island is a lagoon (8.5 km x 3.2 km) with the primary inlet along the north face of the island. The atoll consists of shallow reef until approximately 20 m depth, after which the slope steepens, exceeding 40° to depths of ~200 m to the north and >1000 m on all other slopes. The north face of the atoll is lined with a lipped gully at approximately 65 m depth, referred to as 'Manta Alley' due to regular sightings of manta along that specific bathymetric feature. Note that Egmont is a spatially distinct atoll separated from surrounding bathymetric features by deep water; however, the relative proximity of Great Chagos Bank raises the potential for remotely generated processes to propagate into the area surrounding Egmont and onto its submarine flanks.

2.2 - Oceanographic Instrumentation

The primary oceanographic measurements presented in this paper were obtained from three sets of moorings deployed along the north face of Egmont Atoll. The first site consisted of a pair of moorings deployed in central Manta Alley (Manta Alley – Central); the second site (Manta Alley – West) featured a mooring located to the northwest at the boundary of Manta Alley and Ile De Rats, and the third site was further west again at the point where flow exits into deeper water off Ile De Rats (Ile De Rats) (Fig. 2a).

At the central Manta Alley site, one mooring contained a near-bed mounted Nortek Signature (5 beam) 500 kHz acoustic Doppler current profiler (ADCP) housed in an elliptical buoy 2 m above the seabed. To acquire data relating to changes in temperature throughout the water column, temperature sensors were mounted on a second mooring located within 200 m of the ADCP. Since the two moorings are separated by a minimal distance, we consider them as a single entity for the purpose of our results. The mooring locations were selected due to the proximity to the primary lagoon entrance but fortuitously coincided with the location at which manta presence was highest during the period between cruises.

Average currents were monitored during the period between cruises (November 2019 – March 2020, corresponding to 102 days) and estimated from 2 minutes of sampling at 1 Hz every 10 minutes with a 2 m vertical resolution. Additionally, higher resolution burst data (velocity and echosounder) were acquired in 1 m bins at 1 Hz for the first 23 mins of each hour. During March, the ADCP deployed in Manta Alley provided the same average sampling every 10 minutes but also sampled continuously at 1 Hz with a 1 m vertical resolution for 7.4 days.

RBR Solo^{3}T temperature sensors were spaced at various vertical intervals on the nearby taut-line mooring, with the highest vertical resolution at the thermocline to maximise the ability to resolve small-scale overturns associated with internal wave perturbations. Conductivity-temperature-depth (CTD) sensors were located at the top and bottom of the mooring, enabling the calculation of both final resting depth and checking for any significant knock-down of the mooring, in addition to monitoring changes in water properties due to outflow from the lagoon. Temperature sensors logged at 1 Hz resolution, while each CTD sampled at 0.2 Hz.

The Manta Alley – West mooring was approximately 2 km to the northwest of the Manta Alley – Central mooring and comprised a Nortek 400 kHz Aquadopp ADCP sampling in 2 m vertical bins and providing 10-minute velocity averages. Vertical profiles of temperature were obtained from 19 Seabird SBE56 sensors sampling at 1 Hz and spaced at various vertical intervals.

During March, the Ile De Rats mooring was deployed on the northern edge of Ile de Rats in 65 m water depth (Fig. 2) housing an RDI 600 kHz ADCP and 13 temperature sensors.

2.3 - Quality control & Processing

Thermistor (T) data from the subsurface taut line moorings were merged to create a time series of temperature variability over depth. Moorings with variable thermistor spacing were vertically interpolated to common 2 m vertical intervals for any comparative analysis, and data from the slower sampling CTD sensors and the 19 SBE56 sensors were linearly interpolated to 1 Hz to match the sample rate of the RBR SoloT sensors. Data were cleaned using a 2σ median window filter and a 5-point running average.

Data from Nortek Signature series ADCP's was processed using OceanContour for coordinate transformation, cleaning, and quality control on the data. Data correlation threshold was set at 40% due to the challenging nature of the sampling conditions caused by bodies of water with few scatterers as well as a high dynamic range in return signal though the water column. Data from the RDI ADCPs at Ile de Rats were filtered by both signal quality and cut off at a maximum sampling distance. Velocity data were filtered using a running mean window in both dimensions. Data were averaged into 10 second ensembles to reduce susceptibility to random noise.

2.4 - Frequency domain analysis

Tidal analysis of currents at the central Manta Alley mooring are based on continuous 10-minute average velocities calculated over 2 m vertical bins. Tidal decomposition was performed using the U-Tide toolbox (Codiga, 2011) and tidal constituents selected as defined in Foreman (1977). Tidal velocity reconstructions were calculated for each ADCP depth bin, excluding any constituent with a signal-to-noise ratio < 2. These predictions were then used to remove the periodic velocity signal, associated here with the barotropic tide, to isolate any non-periodic signals which may be associated with baroclinic motions.

To characterise the variance in the observed currents due to periodic, deterministic signals, power density spectra were computed for each ADCP depth bin. The temporal variability in power spectra was further evaluated by use of wavelet analysis using a continuous Morse wavelet transform.

2.5 - Vertical current shear and water column instability

Assessment of the susceptibility of the water column to overturning and mixing by shear instability, which is frequently invoked as a dynamical impact driving a biological response throughout the ocean (Mahadevan, 2016; Hosegood *et al.*, 2019), was estimated by the Richardson number, $Ri = N^2/S^2$ where $N^2 = g/\rho_0 \; \delta\rho/\delta z, \rho_0$ is a reference density taken as the depth mean density from a CTD profile taken in Manta Alley, and $S^2 = (\delta u/\delta z)^2 + (\delta v/\delta z)^2$where u and v are eastward and northward velocities, respectively. Instability is expected for periods where Ri < 0.25, theoretically leading to the development of Kelvin-Helmholtz billows within which vertical overturns are generated and that manifest themselves as temperature inversions. Density estimates for N^2 were calculated for the moorings by assuming a constant T-S relationship; a mean salinity profile was calculated from two CTDs on the mooring (top and bottom) that demonstrated a minimal variation in salinity (<0.05 PSU standard deviation over the calculated period at each CTD). Temperature was measured through throughout the water column by the thermistor string, and density estimated using the TEOS-10 expression for in-situ density (Roquet *et al.*, 2015). Due to the dominance of temperature in driving density gradients in the water column at this site with little freshwater input, the use of a static salinity for time series Ri calculations is expected to result in only a small underestimate of the density variability (Leichter *et al.*, 2012). CTD profiles were vertically binned at 0.5 m for temperature, salinity, and pressure to compute density.

2.6 - Remote sensing & numerical model output.

The IOD index used in this work is provided by the Ocean Observations Panel for Climate (OOPC) Dipole Mode Index data series, which in turn is calculated from the monthly sea surface temperature difference between the tropical western Indian Ocean, and topical eastern Indian Ocean as defined in Saji *et al.* (1999) using the Reynolds OIv2 SST analysis. A shorter timescale of variability (1-2 months) arises through the influence of the Madden-Julian Oscillation, for which the daily index values at 70° E are taken from the Climate Prediction Centre (Xue, Higgins and Kousky, 2002). The MJO is responsible for the enhancement of westerly winds that may potentially promote nutrient entrainment into the euphotic zone and increased rainfall that may increase upper ocean stability but also elevate run-off of nutrients from atolls host to bird populations (Graham et al., 2020)

Local wind data is taken from the ERA5 delayed ECMWF reanalysis (10.24381/cds.adbb2d47), which was cross compared to in-situ met station observations for validation. To evaluate the wider scale influence of the IOD on the thermocline within the central Indian Ocean, the numerical model output from the Copernicus Global Ocean reanalysis (10.48670/moi-00021) and forecast (10.48670/moi-00016) were taken at 1/12° resolution with interpolated depth bins at 5 m increments for improved resolution of the thermocline depth. Remote Chl-a data are taken from the Copernicus global biogeochemistry hindcast at 1/4°with a monthly time step (10.48670/moi-00019).

3 – Dynamical oceanographic drivers of temperature heterogeneity

Given the local topography, candidate mechanisms for the generation of near bed cooling implicated in manta foraging include internal (tidal) waves (Thorpe and Lemmin, 1999; Williams *et al.*, 2018; Reid *et al.*, 2019) as well as the generation of cold water fronts by flow topography interaction (Lü *et al.*, 2010). Internal waves propagate within the ocean interior within the frequency range $f < \sigma < N$, where $f = 2\omega \sin\theta$ is the local Coriolis frequency determined by earth's rotation rate ω at latitude θ (herein taken as 6.55° S). Upon interaction with topography, the evolution characteristics of internal waves are primarily governed by the relationship between the slope of the internal wave, and the slope of the topography. The slope of an internal wave is given by:

$$s = \sqrt{\frac{\sigma^2 - f^2}{N^2 - \sigma^2}} \qquad [1]$$

where σ is the forcing frequency of the internal wave. When the bed slope is shallower than the wave slope, the bed is deemed subcritical, and slopes steeper than the wave face are deemed supercritical. By this classification most slopes in the region are supercritical with respect to the internal tide, meaning that the majority of energy in the internal tide is reflected into deeper water (Müller and Liu, 2000) rather than, in the subcritical case, reflected further up the slope. The propagation of waves obliquely to the slope, however, can reduce the effective angle of the slope, allowing for the upslope propagation of internal waves in cases where the steepness is prohibitive of perpendicular propagation (e.g. Hosegood and Van Haren, 2004).

Local generation of internal tides by topography is governed by the body force function where the baroclinic internal tide is generated by the vertical motion induced by the interaction of the barotropic tide with sloping topography (Baines, 1973):

$$w(x,z,t) = -Qz\left(\frac{1}{h}\right)_x \cos\omega t \qquad [2]$$

Where the mass flux (Q) is determined by changes of bed height (h) in the cross-slope direction (x), and where ω is the tidal forcing frequency and $w(x,z,t)$ is the vertical velocity. This means that, in the case of Egmont, a cross-shore velocity component is necessary for local internal wave generation given the small depth gradients in the along-slope direction in Manta Alley (Fig. 1). Prior studies (e.g. Haury et al., 1979; Lamb, 2004) have identified the role of tides in generating these cross-slope currents which in turn may generate internal waves and vertical excursions of the thermocline which manifest as near bed reductions in temperature.

In the presence of strong and continuous stratification and steep bottom slopes, the predominantly mode-1 internal wave response from (tidal) flow-topography may become more complicated by the generation of a mode-2 response (Vlasenko and Alpers, 2005; Liang *et al.*, 2018; Liu, Grimshaw and Johnson, 2019). Mode-2 internal waves have received significantly less attention than mode-1 internal waves that are dominant in (approximately) two-layer systems in which two weakly stratified layers are separated by a discrete pycnocline of finite thickness. Mode-2 waves are characterised by a divergence in isotherms and strong vertical shear across distinct layers that alternatively drive water upslope and downslope. Mode-2 waves have recently gathered traction as a mechanism for inducing mixing across the pycnocline due to their potential for promoting instability, and thus turbulence (Carr *et al.*, 2019).

The depth at which internal wave effects are pronounced depends on the regional stratification. Strong positive IOD events result in a deeper thermocline within the archipelago and negative events cause shoaling of the thermocline (Liu *et al.*, 2022); the timescale and strength of the IOD varies, although recent years have shown an increased in bias towards positive events (Abram *et al.*, 2008; Du *et al.*, 2020). The modulation of the thermocline by these processes will in turn determine the depth band which any internal wave activity within the region impacts.

4 - Results

4.1 – Near bed cooling on the north face of Egmont Atoll: An overview

As previously described, the north face of Egmont Atoll features a lipped gully referred to as Manta Alley that runs along-slope and, under certain conditions, is inundated at the bed with cold water. While cooling is observed at all three sites (two within MA and one at IDR), the vertical extent of cooling at the Manta Alley – Central mooring is reduced relative to the other two sites. For example, at 11/03/2020 when 26 °C water Is seen to extend to ~30 m depth at Ile De Rats, the same cooling does not extend shallower than ~40 m within central Manta Alley (Fig. 3). Additionally, over extended time periods the variation in thermocline depth plays a central role in governing the depth range over which cooling events are observed.

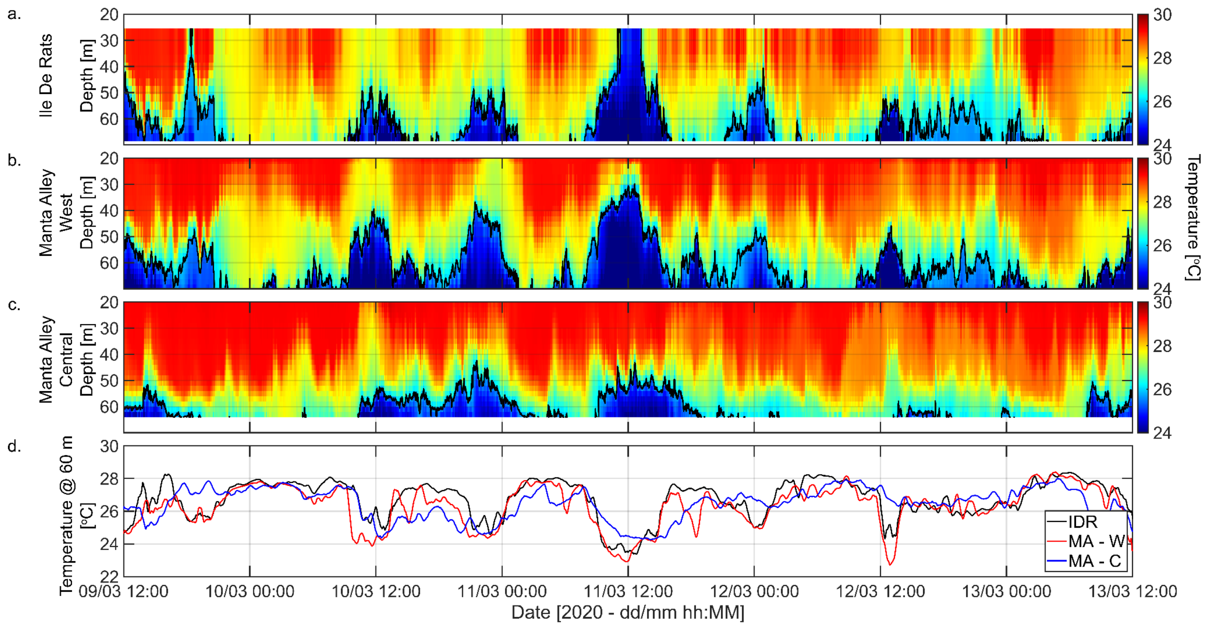

Fig. 3. Temperature at the three moorings located along the north face of Manta Alley in West-East order: a) Ile De Rats: March 2020 mooring (IDR) b) Manta Alley – West: long term mooring to the east of the Ile De Rats 2020 mooring (MA – W) and c) Manta Alley – Central: long-term mooring close to the primary entrance to the lagoon (MA – C). Panel d) shows the temperature at 60 m for each of the moorings to aid in highlighting the variability between sites. Thermistor data overlaid with 26 °C contour.

With the aim of exploring how the differences in these cold-water intrusions may be responsible for the spatial variability in manta residence, the following sections each explore a specific periodicity to examine in further detail how these cooling events are influenced by the local and regional dynamics at three temporal scales:

S 1—Regional stratification (controlled by the IOD) determines the absolute vertical limit to which cooling can extend by varying the depth of the thermocline which support the propagation of processes such as internal waves; the regional impact of the IOD further implies an influence over a significantly wider region than Egmont or the Chagos Archipelago

S 2 – Local tidal period cold water intrusions are regularly seen near the bed at both Ile de Rats and Manta Alley; the similar timings of the events at both locations are suggestive of cooling which propagates up-slope despite the along-slope alignment of the barotropic tide.

S 3 – Baroclinic currents introduce further variability to the local cooling events; observations of high frequency (T < 30 mins) internal waves coincide with rapid cooling at the bed in addition to the tidal period cooling, as well as introducing elevated levels of shear near the bed.

<u>4.2 – Seasonal modulation of background stratification & currents</u>

November 2019 saw an historic peak in the strength of the positive phase IOD (Fig. 4), driving a sustained intensification of the easterly wind fields in the western Indian Ocean and a deepening of the thermocline to > 100 m throughout the archipelago (Lu and Ren, 2020). Modelled results indicate a suppression of the local wind field (Fig 4.) and a depression of the 26 °C isotherm to 120 m in deep water to the east of the archipelago in 2019 compared to 85 m at the same time in 2018 (Fig. 5).

The MJO has a shorter period than the IOD, varying over timescales of 30 – 60 days. Both cruises captured a transition in the MJO, from positive to negative in November, and negative to positive in March. Locally observed wind was not clearly impacted by these transitions, but the stability of the wind field over this period may be in part due to the relative strength of the IOD suppressing the impacts of the MJO (Fig. 4).

The relaxing of the IOD between November 2019 and March 2020 into a neutral phase materialises in the water column as a shoaling of > 35 m of the 26 °C isotherm (a proxy for the top of the thermocline) (Fig. 5). In situ observations corroborate this change with CTD profiles taken in November 2019 and March 2020 showing the 26 °C isotherm migrating from 104 m to 63 m. This initially results in limited opportunity for cooling events during November 2019 within Manta Alley as any internal waves in the region are limited to depths inundated by the thermocline. As the IOD relaxes throughout the end of 2019 and into early 2020, the shoaling of the thermocline facilitates the introduction of cold water at shallower depth bands and, specifically, into Manta Alley (Fig. 6). Data collection in March 2020 took place in comparatively neutral phases of the IOD with shallower accompanying thermoclines at ~60 m and increased observations of near bed cold-water incursions into Manta Alley.

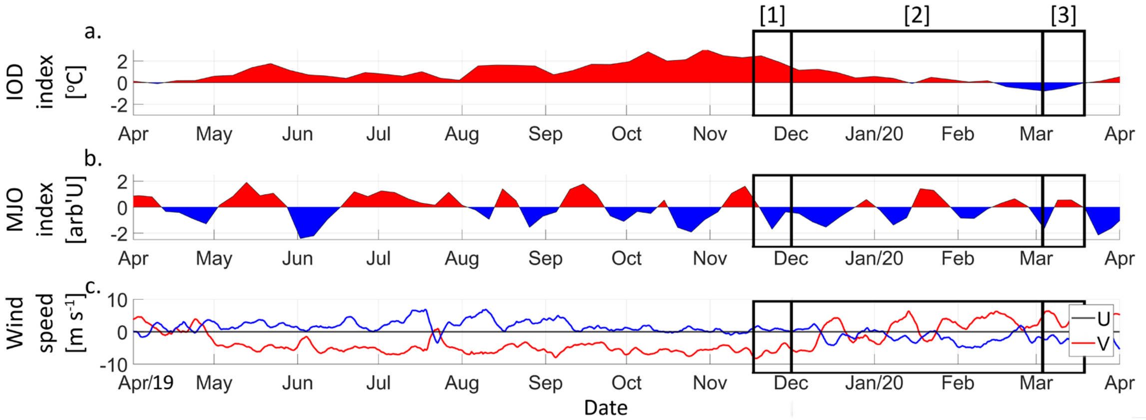

Fig. 4. a) Evolution of the IOD (via. DMI) and b) MJO (via. MJO index at 70E) between September 2019 and March 2020 showing the occurrence of an extreme positive IOD event. c) ERA5 Wind data at 6.75° S 71.25° W showing the suppression of wind variability during the strong positive IOD phase. Indicated are the three observational periods in Nov 2019 [1], over the long-term period [2], and in Mar 2020 [3]

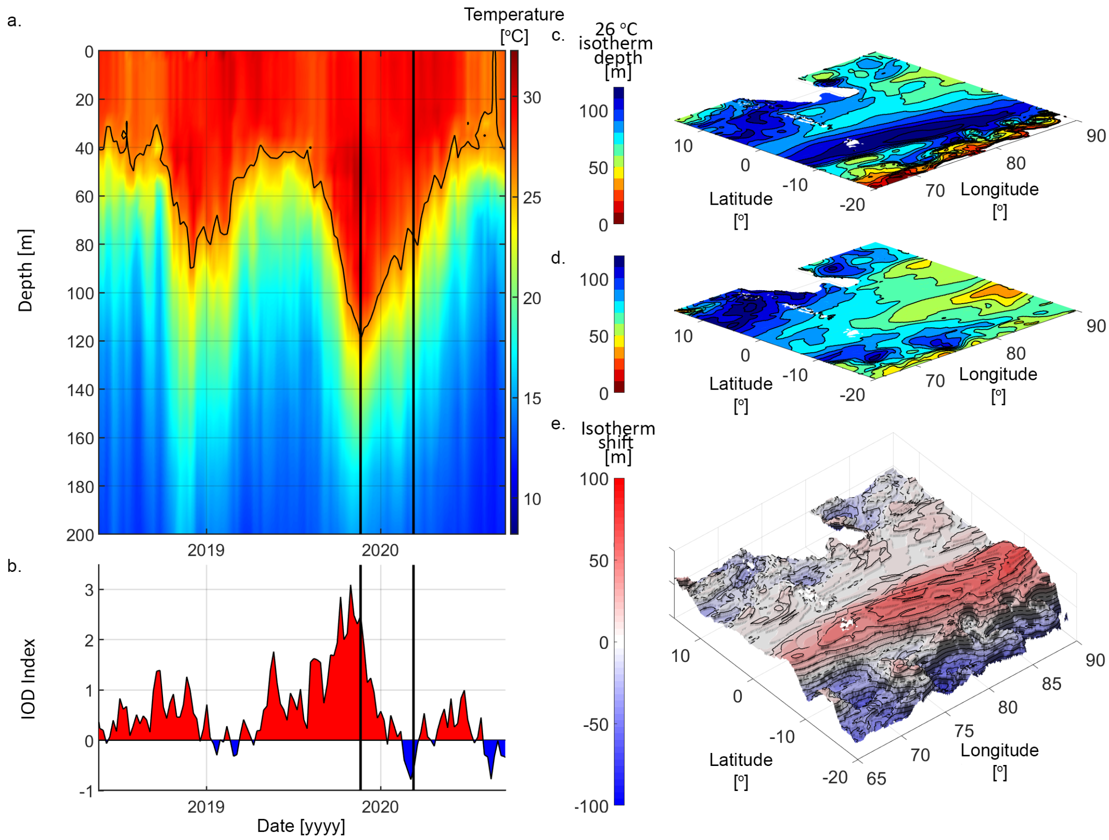

Fig. 5. (a) Modelled (Copernicus) time series of temperature at -8.125 N 73.875 E with cruise timing marked. (b) IOD index provided by OOPC. Spatial position of the 26 °C isotherm is shown over the archipelago between (c) November and (d) March to generate (e) a difference map [November 2019 – March 2020] with positive values indicating a shoaling of the thermocline over the period. Over the region encompassing the Chagos Archipelago, the 26 °C isotherm is 40-50 m shallower during March than in November.

At the Manta Alley – West mooring (which was deployed for an extended duration and features the deepest observations out of the three sites) the gradual shallowing of the thermocline can be seen between December 2019 and March 2020 in response to both the relaxing of the IOD and the standard seasonal evolution, which corresponds well with the remotely sensed / modelled data seen in Figure 5a. Initially, in November the mixed layer base was deep enough (at ~100 m) to exclude monitoring of the thermocline by the moorings, which had maximum depths 65 m (MA) and 75 m (IDR). As the IOD relaxed, the thermocline shoaled and moved into the observable range of the instrumentation (Fig. 6). The date of initial observation for cold water at the bed, defined here as a 2 °C difference across the mooring range, Δ T, on the Ile De Rats mooring was 05/12/2019, and by 31/12/2019 > 25 % of profiles in any given 24 h window exhibited a Δ T > 2 °C over the vertical extent of the mooring.

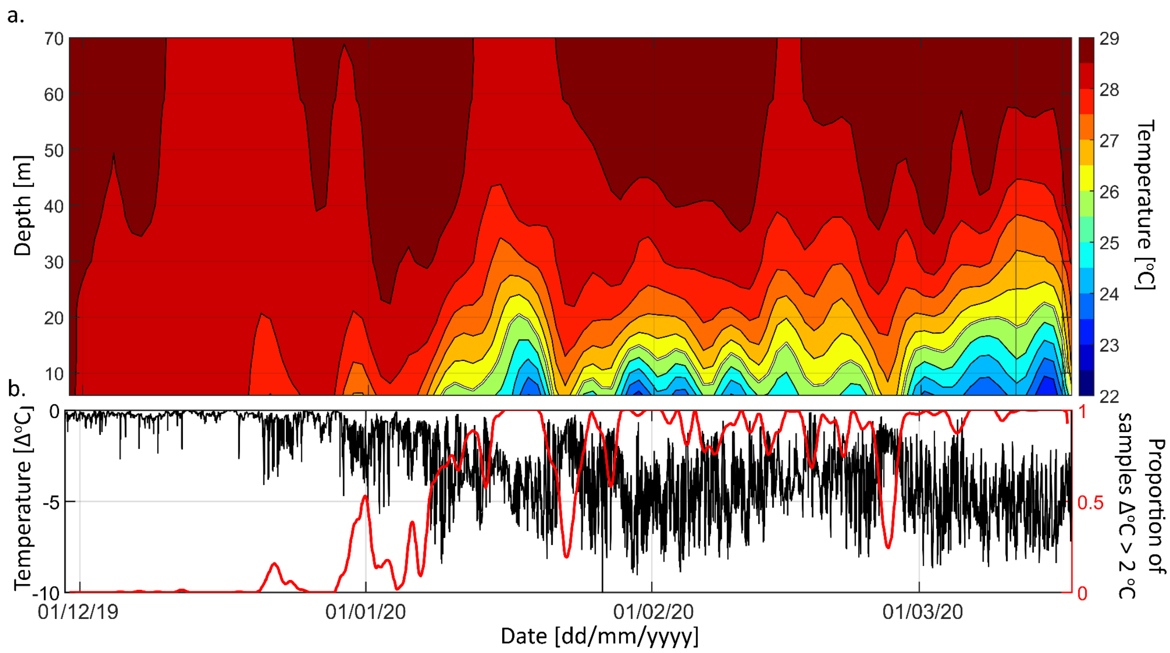

Fig. 6. a) Long-term thermistor data from Ile De Rats showing the evolution of the thermocline depth. 0.5 °C interval isotherms overlaid with 26 °C isotherm shown in white. b) Surface (10 m depth) and near bed (77 m depth) temperature difference [black] and proportion of 5 min samples with a difference greater than 2 °C [red, 201 point running average] over the course of the long-term mooring deployment at Ile De Rats.

Due to the presence of a DCM within the Indian Ocean, the seasonal migration of the thermocline also resulted in vertical migration of the DCM. Comparing the hindcast data for Chl-a in November 2018 and 2019 (Fig. 7), it is apparent that the 60 m depth band (the depth at which the majority of Manta Alley lies) was comparatively depleted of Chl-a in 2019 compared to a more historically representative year in 2018. Comparatively, at 100 m during 2019 there were higher Chl-a concentrations suggestive of a DCM migrating with the thermocline which was a consistent feature from in-situ CTD profiles taken during this period. These profiles show Chl-a concentrations at the thermocline of 0.82 µg L^{-1} compared to < 0.2 µg L^{-1} in the top 20 m of the water column (Fig. 7). This coupling of the thermocline with the DCM is a key element of the biophysical coupling that allows for physical oceanographic processes to influence local ecosystems, particularly via internal waves propagating along the thermocline.

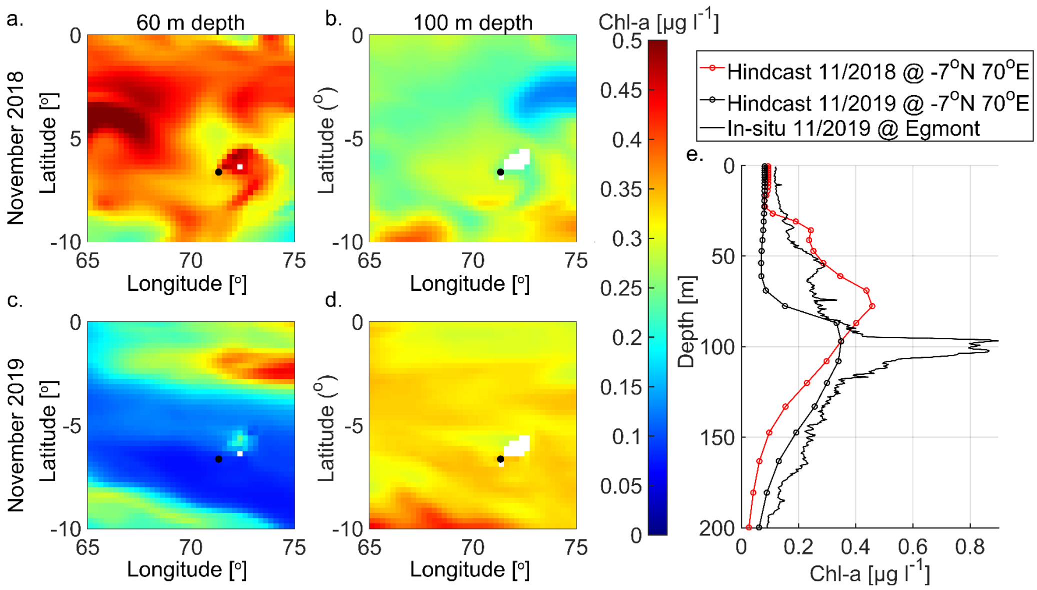

Fig. 7. Chl-a concentrations at 60 m and 100 m depth from the global ocean biogeochemistry hindcast in 2018 (a, b) representative of a standard depth thermocline and 2019, (c, d) with the thermocline deepened by the IOD. Egmont is marked by the black dot, visible is the comparatively depleted Chl-a at the depth of Manta Alley in 2019. e) Profiles of Chl-a from both scenarios in deep water to the south-west of Egmont, along with an in-situ profile taken in deep water off Egmont in November 2019.

4.3 – Local Tidal Forcing

The tide is mixed and asymmetric within Manta Alley; the magnitude of the solar diurnal (K_1) component is equal to that of the lunar semi-diurnal (M_2) component (Fig. 8). Semi-major axes amplitudes are 0.111 m s^{-1} (95 % confidence interval [CI95] 0.006) and 0.097 m s^{-1} (CI95 0.007) for K_1 and M_2, respectively, with a similar ratio of M_2/K_1 currents to that reported previously at the nearby more exposed Sandes seamount by Hosegood *et al.* (2019). Currents are forced to align locally along-slope, resulting in rectilinear current ellipses (Fig. 8a) both within Manta Alley and around the wider atoll following the underlying isobaths (Fig. 9). Within Manta Alley the flood tide runs eastwards, and the ebb tide runs westwards. The minimal local cross-shore current implies a low likelihood of local internal tide generation due to the requirement of flow over slopes for IW generation in the body force function as shown in eq. 2.

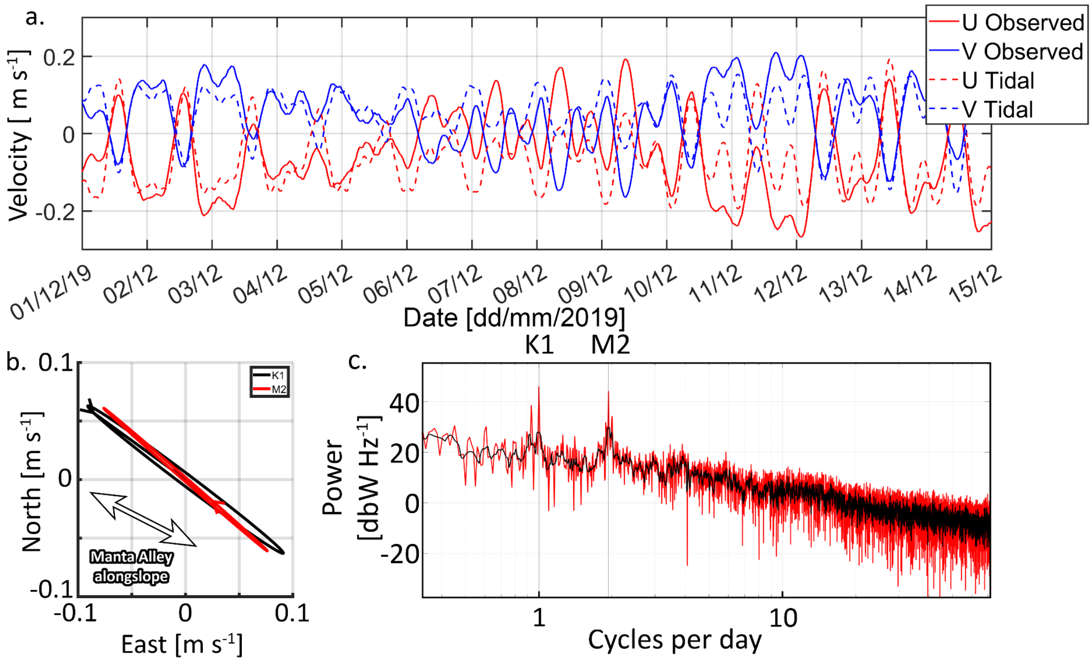

Fig. 8. a) One month of observed currents in Manta Alley overlain with predicted tidal velocities from tidal decomposition analysis. b) Depth-mean tidal ellipses for the K_1 and M_2 components over the period of long-term observations taken from within Manta Alley. Within Manta Alley the magnitude of the K1 component matches that of the K2, not visible within the ellipse is the asymmetry in the strength of the tidal currents. c) FFT of depth averaged eastwards velocity showing equal powers for the K1 & M2 components

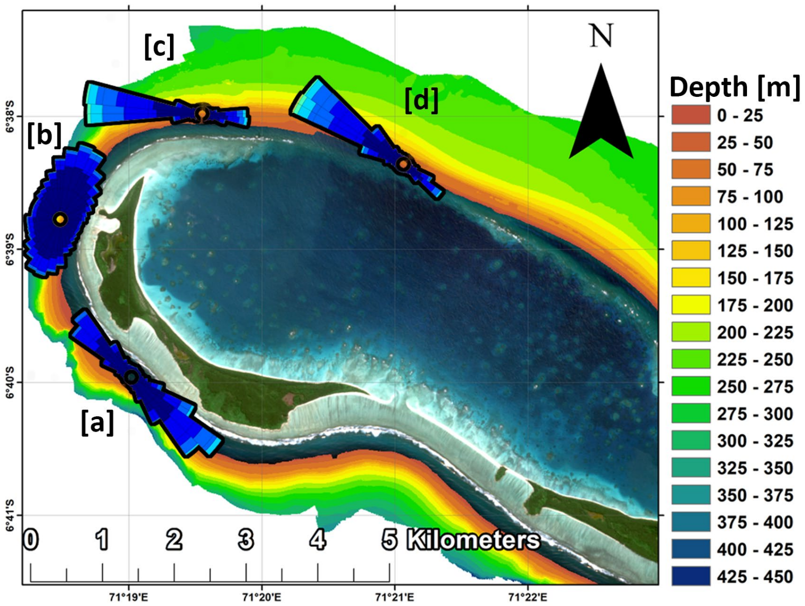

Fig. 9. Current roses inset into bathymetry at Egmont, showing the modulation of current direction by the local bathymetry. Instrumentation was as follows [a] Ile Sepille 1000 kHz ADCP (Nov 19) [b] Ile De Rats (W) 600 kHz ADCP (Nov 19) [c] Ile De Rats 400 kHz ADCP (Nov 19 – Mar 20) [d] Manta Alley 500 kHz ADCP (Nov 19 – Mar 20). Background imagery from Copernicus Sentinel-2B [2022] / Sentinel Hub

4.4 – Barotropic tidal forcing of near bed thermocline incursions

To assess the baroclinic response to tidal forcing over the slopes surrounding Egmont, a subset of data is presented in the presence of the shallower thermocline (March 2020) from Ile De Rats with a 6-hour low pass filter applied to isolate variability at the M_2 periods and above (Fig. 10). Cold water incursions, evident as cold water at the seabed and extending vertically towards the surface, are visible at tidal periods with vertical amplitudes of up to 40 m; these events generate Δ T >8 °C between the bed and 10 m depth over a short period (≈ 5 mins), and 4 °C over the course of a tidal period, compared to a baseline Δ T of ~ 2 °C (Fig. 10). The cooling evident over tidal periods is a persistent feature at diurnal and semi-diurnal frequencies when the thermocline intersects the slope within the observational range. This cooling is likely to be a persistent feature, including in the presence of a deeper thermocline due to the consistency of any tidal forcing, despite being beyond the depth range of our observations that are constrained by the steep slopes offshore of Manta Alley.

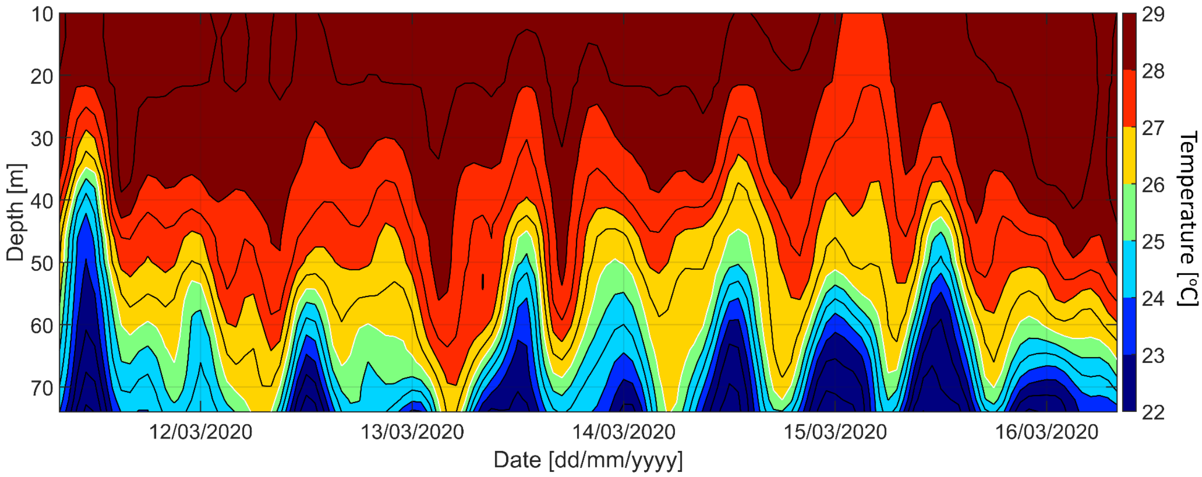

Fig. 10. Long-term thermistor data from Ile De Rats. low passed at 6 hours to remove high-frequency oscillations and isolate the temperature change at the timescales associated with tidal (M2, K1) processes. Seabed at 77 m depth. 0.5 °C interval isotherms overlaid with 26 °C isotherm shown in white.

Despite the tidal currents being aligned predominantly along-slope, the temperature differences that are the subject of this paper appear to be only weakly linked to currents orientated in this direction. At Ile De Rats, along-slope velocity, and the depth of the 26 °C isotherm (chosen as a marker for the base of the surface mixed layer) have a weak linear relationship. Positive along-slope flows (flood tide, eastwards) are associated with shallower isotherms and cooler near bed temperatures. This relationship is weaker at Manta Alley – Central, with the gradient of the linear fit at Ile de Rats being -11, compared to -6.1 at Manta Alley over the same period. This can be seen in figure 11a where the distribution at Ile De Rats shows that the shallowest elevations of the isotherm are predominately associated with strong positive along-slope flows. Manta alley shows a comparatively normal distribution with the shallowest isotherms found during periods of relatively minimal (<0.1 m s^{-1}) velocity as shown by the central distribution in figure 11c.

At Ile De Rats, the measured velocity range was 0.37 m s^{-1} (2σ) and the depth of the 26 ˚C isotherm varied between > 64 m to as shallow as 31 m depth, a range of over 33 m with the shallowest isotherm seen on 13/03/2020, on the flood phase of a spring tide. Velocities at Manta Alley were smaller with a range of 0.28 m s^{-1} (2σ) with the thermocline not reaching depths shallower than 40 m during this period, this is again demonstrated by the reduced vertical and horizontal spread in figure 11c.

The limited corelation between the along-slope velocity, which is primarily driven by the barotropic tide, and the shoaling of the isotherm suggests that a freely propagating internal tide in the along-slope direction is relatively unlikely to be the driver of the observed cooling within Manta Alley. This is further corroborated by cross-correlation between temperature at a depth of 60 m at each site; no time delay is observed between the two signals over the period of observation, despite a horizontal separation distance > 1 km.

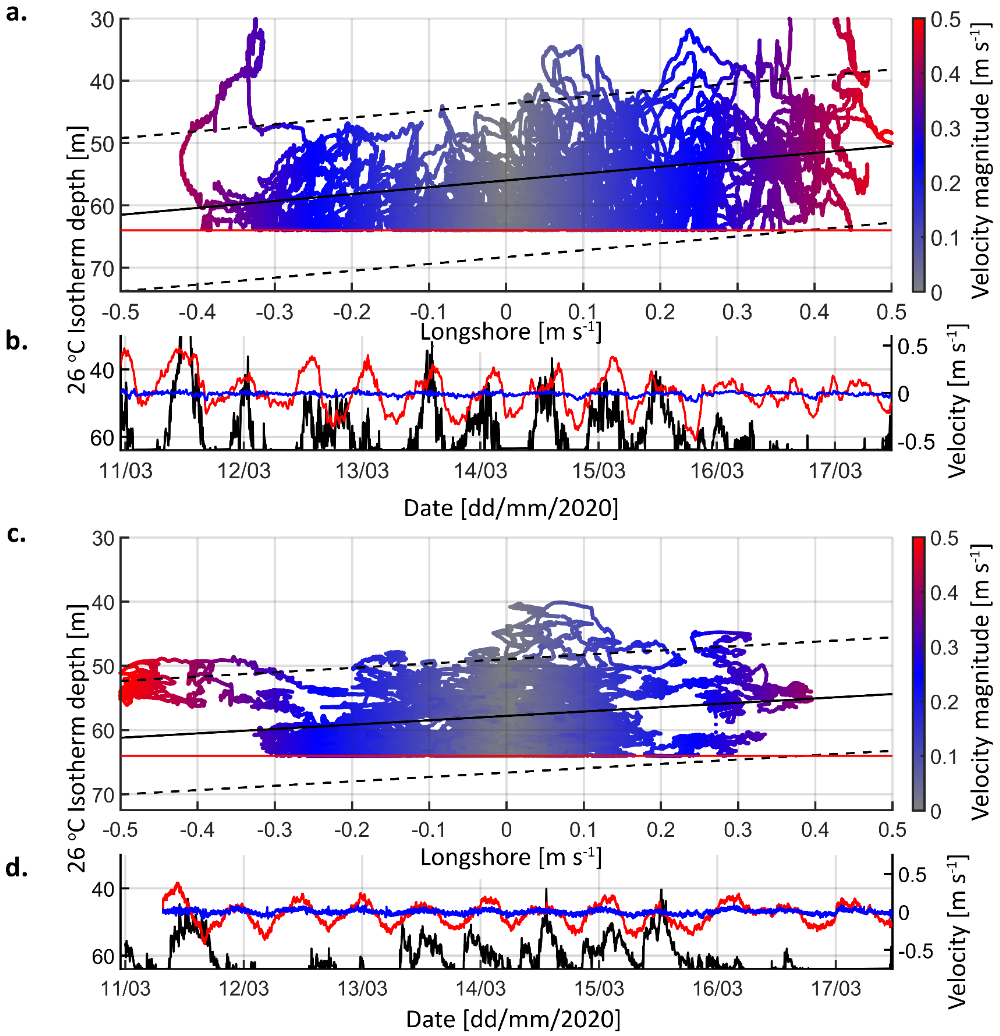

Fig. 11. Depth of the 26 °C isotherm between 2020/03/10 23:00 and 2020/03/17 11:30 at (a, b) Ile De Rats and (c, d) Manta Alley – Central related to depth mean longshore velocity between 31 & 61 m depth (overlapping observational range). Visible at Ile De Rats is the trend of raised isotherms during eastwards flow and depressed isotherms during westwards flow fitted with the linear regression y = -11.0x + 56.0 ± 12.3 CI95, R 0.11. Longshore [red] and cross-shore [blue] velocities shown with isotherm depth [black] with clear correlation between the peaks in cross-shore velocity and shallow isotherm. At Manta Alley longshore velocity has limited impact on the depth of the isotherm when fitted with the linear regression y = -6.1x + 57.08± 8.8 CI95, R 0.05. While normally there are weak positive LS velocities with shallow isotherms, the event on 11/03 is out of phase with the background velocity resulting in the block visible to the left of panel c.

4.5 Internal wave generation and propagation

To assess the role of a cross-slope propagating internal tide in generating bed temperature fluctuations at Egmont, the ability of nearby slopes to generate internal tides was calculated. The background stratification is strong, with temperature gradients up to 1.4 ˚C m^{-1} observed in November 2019 and 0.5 ˚C m^{-1} in March 2020 and peak N^2 values exceeding $4x10^{-3}$ s^{-2} in 2019. The range of observed N^2 values (Fig. 12) indicate that internal waves forced by the M_2 tide in the vicinity of Egmont would have a peak slope of approx. 3.5° in the strong stratification found in November 2019. The local slope at Egmont regularly exceeds 30° (Fig. 2) and is therefore supercritical to the slope of semi-diurnal tide forced internal waves within the region (Balmforth and Peacock, 2009).

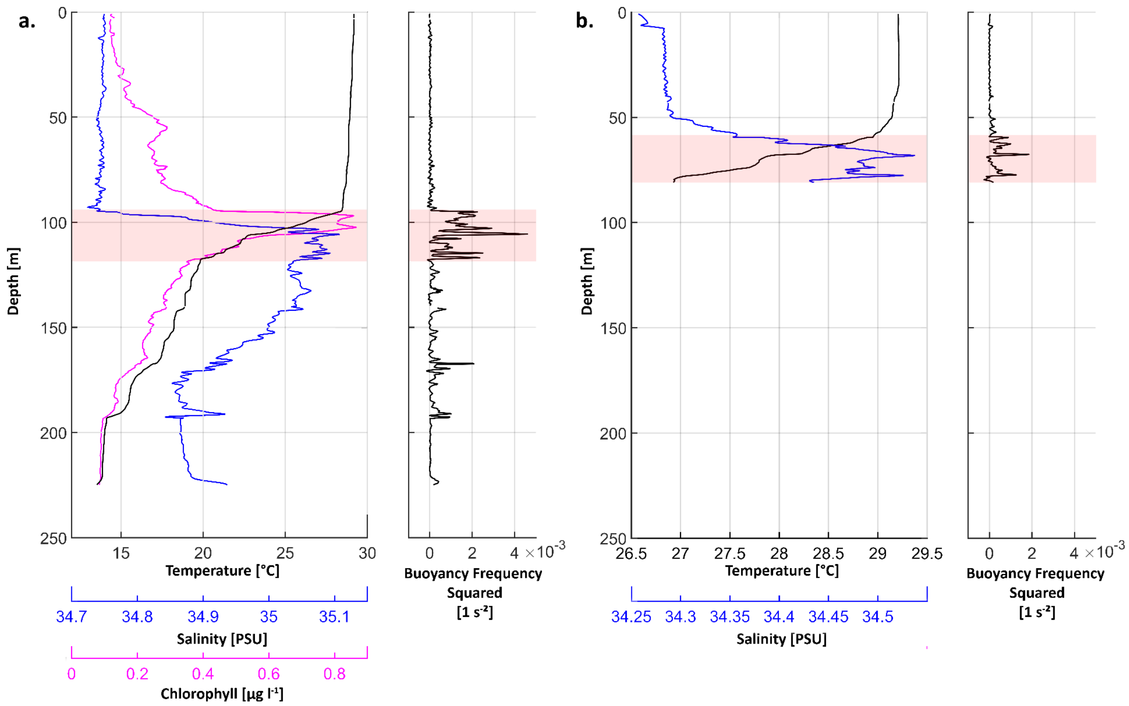

Fig. 12. In-situ Temperature, Salinity, Chlorophyll profiles at Egmont from a) November 2019 and b) March 2020 showing the shift in stratification along with accompanying N^2 values for the profiles showing increased buoyancy frequency at the thermocline. Note differing horizontal scales due to vastly different prevailing conditions. The region of peak stratification (associated here with the thermocline) has been shaded.

4.6 — Baroclinic dynamics: High frequency internal waves and cooling events outside the barotropic tidal regime

Cooling events at Egmont are not exclusively phase-locked to barotropic tidal forcing but appear, on occasions, at irregular intervals resulting in variations of the cooling signature between each occurrence (Fig. 11, 13). To elucidate the dynamics controlling these apparently non-tidal events, and to demonstrate their turbulent nature, an example case is shown with two tidal periods exhibiting vastly different characteristics; the first period commencing on 14/03/2020 20:00 shows weaker stratification with a 5-15 m vertical separation of isotherms at 1 °C intervals, whilst the second on 15/03/2020 09:00, shows strong stratification and the presence of colder 20 °C water at the bed. Data are presented with the barotropic tidal velocity from the tidal analysis removed to better highlight the local baroclinic forcing.

During the first event a residual along-slope current amplitude of 0.5 m s^{-1} was observed between 10 and 30 m above the seabed, with an associated decrease in temperature of 4.2 °C, from 26.3 °C to 22.1 °C, measured 2 m above the seabed with a peak rate of 0.28 °C per minute (measured over a 5-min window). The barotropic velocity of ~ 0.5 m s^{-1} was opposed by the baroclinic component responsible for the cooling, resulting in an observed current of effectively 0 m s^{-1}. This cooling persisted for a duration of 4.5 h before the thermocline returned to depths below the mooring (Fig. 13.).

The baroclinic component exhibited significant vertical shear (Fig. 13a.), as well as an enhanced cross-shore component with velocities up to 0.2 m s^{-1}. The cross-shore component is oscillatory at short time scales (15-30 mins) associated with the presence of high frequency variability in isotherm depth accompanying the tidal carrier wave (Fig. 13 b,c). Vertical velocities are generally below 0.05 m s^{-1} with the strongest vertical velocities found at the bed on the leading edge of the 09:00 event. The near bed cold water incursion is constrained to the vertical layer in which the residual current is strong and aligned along-slope, with an increased residual cross-shore component compared to the warmer surface water.

A high concentration of scatterers within the upper edge of the thermocline can be seen for the duration of the cooling event, with a separate body of highly clear water below this scattering layer (Fig. 13f). Without ground truthing it is not possible to definitively establish the cause of these scatterers, with potential sources being sedimentary, biological, or turbulence based (Muchowski *et al.*, 2022). The presence of cold clear water below this high intensity band is, however, suggestive of either a plankton layer which has been vertically advected into the alley or reflections of stratified turbulence generated by the shear across the interface.

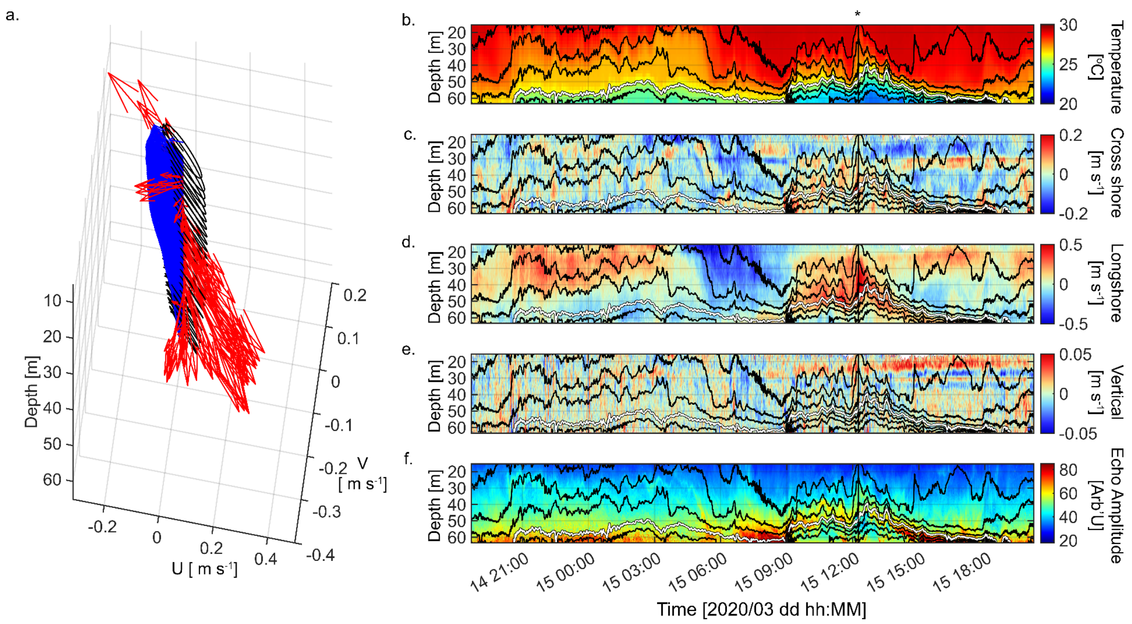

Fig. 13. a) K1 Tidal ellipses (Black) with instantaneous predicted tide quivers (Blue) and residual current quivers (Red) overlain and showing a cross-shore component near the bed. b) Temperature, c) baroclinic cross-shore velocity, d) baroclinic longshore velocity, e) vertical velocity, and f) echo amplitude from the Manta Alley – Central mooring showing two consecutive tidal periods which display different cooling characteristics. Seabed at 66 m. Panels b-f are overlaid with temperature contours at 1 °C intervals (29 – 23 °C) with the 26 °C shown in white.

During this event, cooling is also observed at the other two moorings to the west; in this case at 60 m depth the cooling appears first at central Manta Alley at approximately 08:57 followed by western Manta Alley at approximately 09:15, 18 minutes later, suggesting that this event may be propagating obliquely to the slope. A further delay can be seen before a weakened cooling signal is seen at the Ile De Rats mooring, further to the west (Fig. 14)

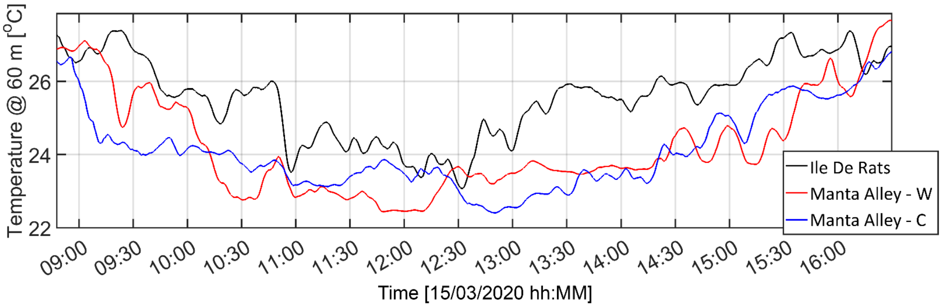

Fig. 14. 60 m temperature at three moorings on 15/03/2020 (Ile De Rats, Manta Alley - West, and Manta Alley – Central) showing a short delay in the appearance of cooling at the three sites, as well as generally weaker cooling at the westmost (Ile De Rats) mooring.

Whilst most observations of subtidal frequency internal waves at Egmont were in the presence of a larger, tidal, carrier wave, there were limited examples seen of isolated trains of high frequency internal waves near the bed, one of which is presented below. In this case there is an associated temperature drop of 3 °C observed at the mooring, with the level of cooling subsiding rapidly after the passing of the wave. These high-frequency waves have short periods between 5 & 10 mins (where local N in the region limits the lower period to approx. 4 mins) and exhibit the elevation-depression vertical velocity pattern characteristic of nonlinear internal waves. This vertical velocity signal peaks at 0.1 m s^{-1} during the first wave at 07:05 and 0.2 m s^{-1}. The lack of corresponding drop in temperature at Ile De Rats, and the strongly cross-shore direction of the flow within the wave, which flows south-westwards with shear at the wave interface between 0.4 and 0.5 m s^{-1} (Fig. 15) both suggest that this may be an upslope propagating wave.

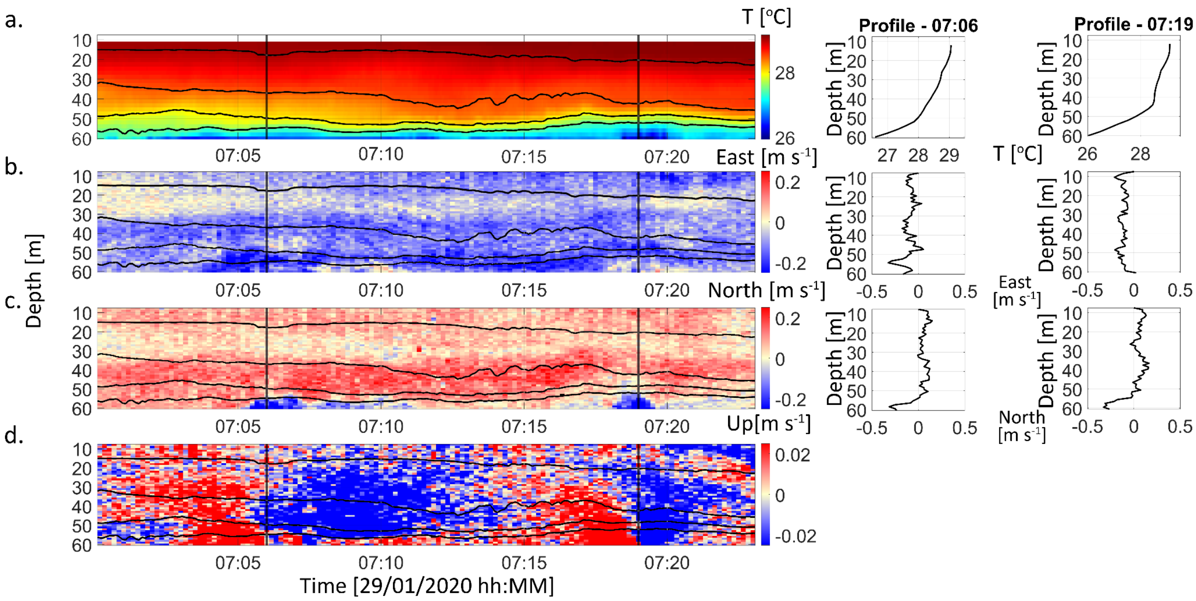

Fig. 15. Spilling of an upslope propagating internal wave into Manta Alley, bringing a cooling of 3 ˚C and resulting in turbulent mixing across the thermocline from high levels of shear at the interface a) Temperature + (b) East / (c) North / (d) Up Velocity Panels with isotherms overlaid at 1 °C intervals.

4.7 Enhanced mixing through internal wave activity generated shear instability.

The shear associated with the near bed propagation of the internal waves shown in section 4.6 is likely to enhance turbulent mixing through shear instability, a metric which can be quantified by Ri. In the example presented in figure 16 (covering the same period shown in fig. 13) two tidal periods were observed with near bed cooling signatures that generate mixing through shear instability. The first period on 14/03/2020 shows weaker stratification, however over the zone of peak stratification enhanced shear was observed. On the trailing edge of the cooling at ~ 15/03/2022 05:00 in the presence of high frequency internal waves the observed Ri values are subcritical (Ri < 0.25), likely due to the stabilising influence of the strong stratification ($N^2 > 1x10^{-5}\ s^{-2}$) (Fig. 16b).

During the second event, vertically banded shear is visible within the core of the wave, with the interface of the tidal period wave exhibiting S^2 values orders of magnitude larger than the background water column, with values of $1x10^{-5}$-$1x10^{-4}\ s^{-2}$ in the background water column, and values in excess of $1x10^{-3}\ s^{-2}$ at the interface of the wave. These waves are associated with reductions in Ri but not always to the point of instability. Shear instability is primarily visible on the leading and tail edges of the short period waves, suggesting that these features enhance mixing across the boundary of the tidal period cooling. During the wave at 12:00 internal instability is also apparent within the lower stratification at 42 m depth.

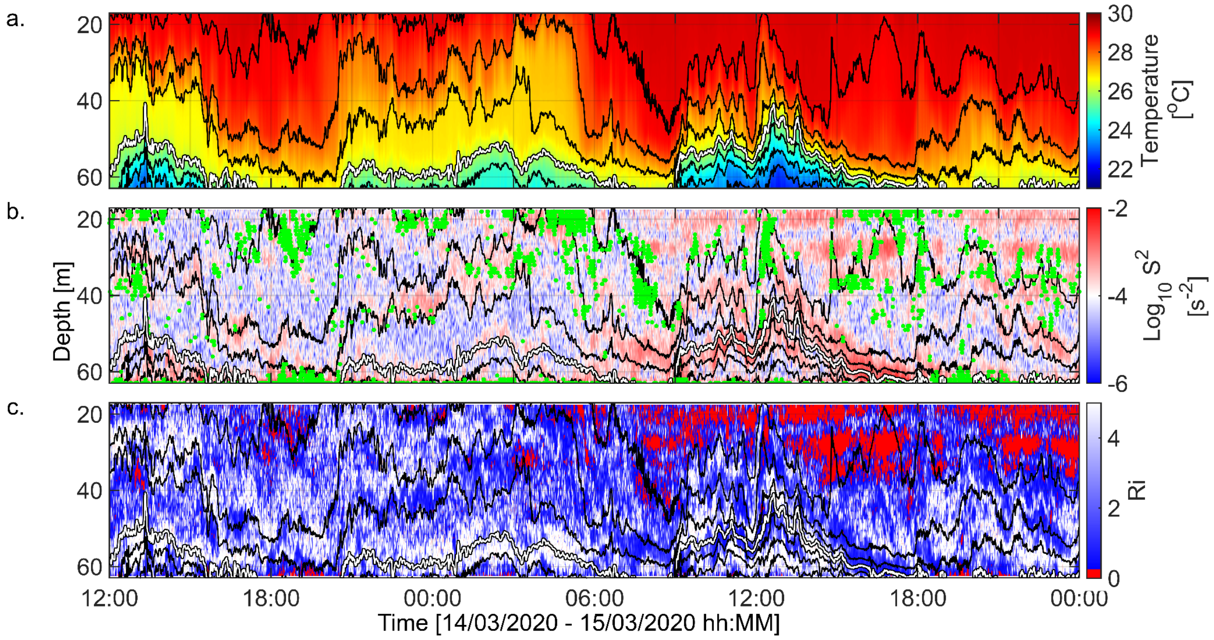

Fig. 16. a) Temperature at the Manta Alley – Central Mooring on 14/03/2020 - 15/03/2020 showing tidal period cooling carrying higher frequency internal waves. b) 2-Dimensional vertical shear overlaid with temperature contours, and areas where Ri < 0.25 & $N^2 > 1x10^{-5}$ *marked in green. c) Ri with highly stable areas marked in white, and zones of subcritical Ri marked in red. Panels are overlaid with temperature contours at 1 °C intervals (29 – 23 °C) with the 26 °C shown in white.*

4.8 – Site specific variability in internal wave activity

The form of the observed cold-water intrusions varies on a case-by-case basis, with the tidal intrusions being the most consistent and high frequency internal wave driven cooling being more site specific. To demonstrate that the cooling observed at both sites, driven by both tidal, and high-frequency internal processes, wavelet analysis was used to highlight the frequencies driving the cooling at a depth of 60 m.

In the initial period spanning 12/2019 – 01/2020, less than 0.3 °C temperature variability was observed, particularly above tidal frequencies (<6h period). The shoaling of the thermocline results in more frequent cold-water incursions, and as such greater thermal variability at each site. In the presence of a shallow thermocline at periods shorter than 12 h, Ile De Rats demonstrates a greater variability of >0.5 °C s^{-2}, indicating that high-frequency fluctuations in temperature are more prevalent at this site (Fig. 17).

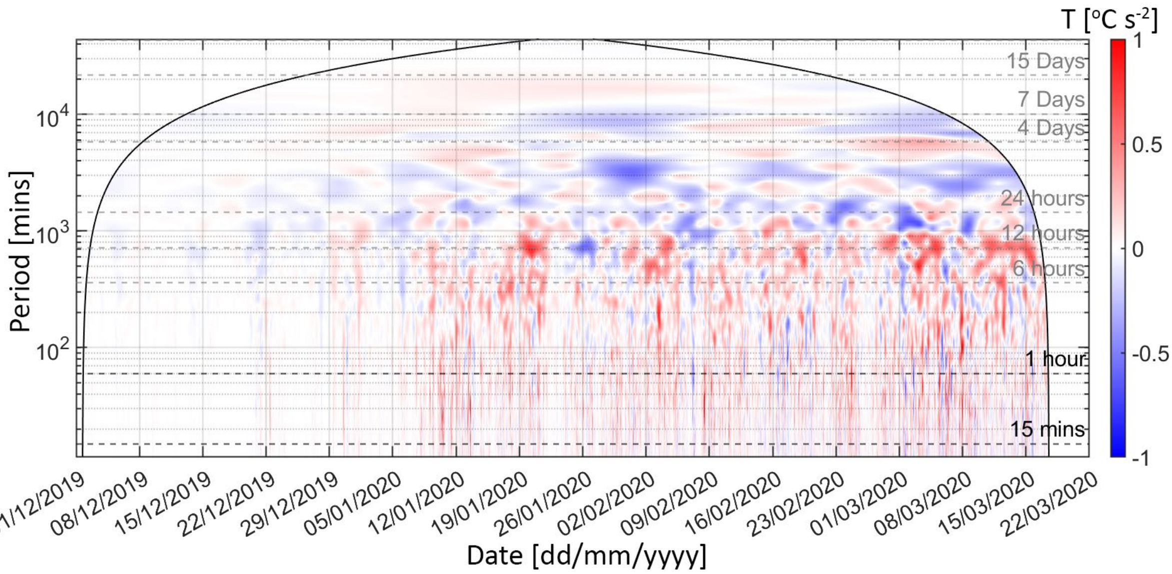

Fig. 17. Wavelet comparison between the long-term moorings in Central & West Manta Alley between December 2019 and March 2020. Areas in red represent periods of higher variance at western Manta Alley, whereas blue areas exhibit higher variance at central Manta Alley. Note the higher energies at high frequencies in the western extent of manta alley (>12h).

A subset of data from March 2020 (Fig. 18.) demonstrates the differences in thermal variability between Ile De Rats and Manta Alley. Both sites are highly active at tidal periods and show a high frequency internal wave signal which is clearly coincident with tidal forcing. This signal is more prevalent at Ile De Rats, with poorer definition within Manta Alley, but the magnitude of thermal variance at shorter periods (T < 1 h) is comparable between the two sites.

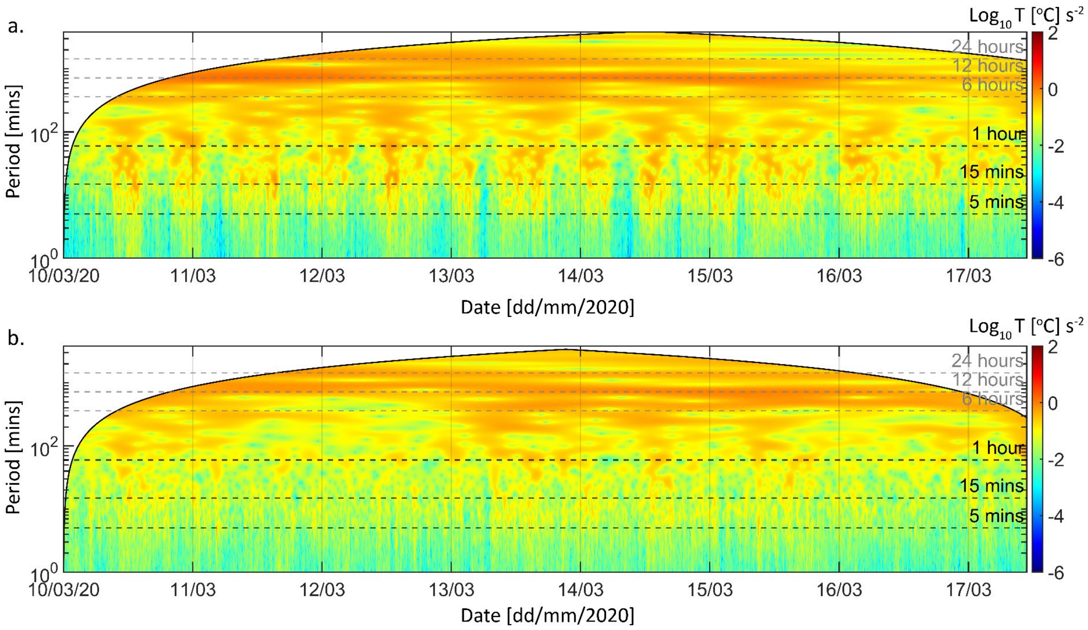

Fig. 18. Wavelet analysis of temperature at 60 m depth at a) Ile De Rats and b) Manta Alley – Central demonstrating the difference in temperature variability between sites over a shorter period but at higher frequencies. Both sites show tidal extension of energy into higher frequencies associated with short period internal waves, however the effect is less pronounced at western Manta Alley.

5 - Discussion

Expanding on the results of Harris (2021) which focused on the impact of temperature on reef manta ray presence/absence at several sites around Egmont atoll, these results show that over short spatial scales Egmont exhibits differences in the thermal regime driven by highly localised physical processes. The temperature changes in Manta Alley are a result of periodic changes to the thermocline depth driven by several mechanisms. At interseasonal time scales the IOD modulates the depth of background stratification; at tidal periods rapid thermal variation is seen, potentially due to an internal tide, and high frequency internal waves drive both shorter period (5 – 15 mins) highly localised cooling events and promote mixing through shear instability in the presence of a tidal carrier wave.

The extreme positive IOD event (Lu and Ren, 2020) resulted in one of the deepest thermoclines, at a depth of ~100 m, seen within the available record. This deep thermocline caused the inundation of features in the 60-70 m range with warm water characteristic of the surface layer, pushing the thermocline too deep for cooling events to be observed in Manta Alley. Previous work examining mass aggregations of manta species have typically suggested that food plays a key role in promoting aggregative behaviour (Armstrong *et al.*, 2016). Manta feed on zooplankton which are in turn dependent on phytoplankton and so to a degree the presence of zooplankton can be inferred by proxy using Chl-a with manta presence previously linked to increased Chl-a levels (Harris *et al.*, 2020). During historic positive IOD events the 40-70 depth band across the entire SCTR in which the archipelago resides showed a decrease in chlorophyll concentrations (Dilmahamod, Hermes and Reason, 2016), and hindcast observations from 2018 and 2019 suggest that the same decrease occurred in 2019.

Due to the large scale of the IOD, impacting on the wider eastern Indian Ocean, many other reefs, atoll, and seamount ecosystems within the 50 -100 m depth band were likely impacted by inundation with warm surface waters at depths typically associated with the cooler thermocline. With climate change driving intensification of the IOD (Abram *et al.*, 2008) the depth range impacted by this variation, as well as the duration for which depth bands may be excluded from cooling is likely to become more extreme.

At local scales, the flow dynamics at Egmont are strongly influenced by the underlying bathymetry, with differences in near bed temperature seen over small distances. The predominant frequency associated with the cooling is semi-diurnal on the flood tide, although the cooling is not exclusively phase locked with the local barotropic tide. The western extent of Manta Alley shows larger amplitude incursions of the thermocline and more activity at the frequency bands associated with short period internal waves. The constraint imposed by the channel to the north of Egmont may cause the generation of accelerated tidal currents despite the small elevation of the tide but, regardless, the changes in oceanographic conditions over small distances indicates the need to adopt approaches that account for the bathymetric complexity at other sites.

Throughout the tidal cycle, cooling events are observed which are consistent with the downstream evolution of mode-2 waves generated by interaction with steep topography in the presence of continuous stratification beneath a weakly stratified surface layer. The generation and lifespans of mode-2 waves is dependent on both the background stratification and shear environments (Chen *et al.*, 2014; Deepwell and Stastna, 2016). Given the difference in stratification observed at Egmont over tidal time scales, this accounts for part of the temporal variability seen. Existing insights into how these waves develop is almost exclusively reliant on the use of nonlinear models (Cheng *et al.*, 2017; Liu, Grimshaw and Johnson, 2019) and so there have been limited in-situ observations of how topography impacts on their evolution.

Considering here that the cooling events are predominantly trapped at the bed due to the proximity of the thermocline to the topography, we typically observe waveforms in which the waves of depression have been potentially suppressed/destroyed (similar to Cheng *et al.*, 2017) or undergone fission and converted to waves of elevation (e.g as in Deepwell *et al.*, 2019). As some of the characteristics of these waves are like mode-1 waves differentiation of the two is challenging. However, the presence of continuous stratification within Manta Alley, as opposed to a two-layer system, and the strong banded shear observed in the waves increases the likelihood of these being mode-2 waves. Additionally a previous study has shown that tidal flow in constrained channels, such as the one between Egmont and Great Chagos Bank, can result in the generation of mode-2 internal waves (Rayson *et al.*, 2018) that likely promote turbulence.

The similarity in timings of the tidal period cooling at both sites is indicative of events which propagate perpendicular to the slope. Recent oceanographic modelling has suggested the presence of an enhanced mode-2 internal tide near the Chagos-Laccadive Ridge relative to the wider Indian Ocean (Zhao, 2018). However, this coarse scale oceanographic modelling (1/10°) is unable to accurately represent the fine-scale bathymetry of the region; at this resolution, Egmont atoll is represented by a single grid point, and bottom slopes are significantly underestimated with GEBCO data showing a peak slope angle of 8° compared to the high-resolution multibeam bathymetry which exceeds slope angles of 40°. The steep bathymetry in the archipelago is widely capable of generating internal tides which may then freely propagate to remote sites such as Egmont, and recent fine scale modelling at Egmont has demonstrated the presence of an arrested mode-2 internal tide in the wider channel between Egmont and Great Chagos Bank due to the local tide being sufficiently strong to arrest the slower, higher mode, internal tide (Diaz et. Al, submitted [unpublished data]).

Any remotely generated internal waves reaching Egmont and propagating perpendicularly to the north face of the atolls are likely to have the majority of energy reflected due to the supercriticality of the local slopes, however the oblique propagation of internal waves presents a mitigation to this factor

(Gemmrich and van Haren, 2002; Hosegood et. al, 2004) meaning that the propagation of remote waves towards Egmont remains a plausible. If these internal tides propagate perpendicular to the north face as suggested by our observations the far side of the atoll is expected to experience reduced cooling compared to the sites on the North & Western faces promoting further dynamical variability over the atoll.

Based on our observations, Egmont displays large thermal variability over even the limited length of Manta Alley. This supports the hypothesis of Harris *et al. (*2021) that fine scale dynamics can have pronounced ecosystem effects which impact on fine scale preferentiality in mobile species. The interaction between diel vertical migration of zooplankton to the DCM, local internal wave dynamics, and topography may directly influence distribution of zooplankton within Manta Alley (Lennert-Cody and Franks, 1999, 2002; A. Cordeiro *et al.*, 2013; Liccardo *et al.*, 2013). Whilst we are unable to directly determine why manta exploit the internal wave-driven events shown here, we hypothesise that the distribution of zooplankton is impacted by the turbulent nature of these dynamics, as seen in motile phytoplankton (Durham *et al.*, 2013), or by fine scale flow fields, and that potentially zooplankton distribution is modified in a manner that assists manta foraging.

Site preferential foraging in response to biophysical processes has already been shown in both manta rays (Couturier *et al.*, 2011; Weeks *et al.*, 2015), and other highly mobile marine species (Jones *et al.*, 2014). As the events are most energetic in Manta Alley, it supports the hypothesis that manta rays are exploiting these features to enhance their foraging efficiency and are detected more often at this location. Further work to validate the relationship between these cold water events and chlorophyll concentrations would provide observational support for the biochemical drivers which may be at play given the lower residence time over the eastern end of Manta Alley (Harris *et al.*, 2021).

6 - Summary

Observations from sub-surface moorings, supplemented with regional remotely sensed data over the period of November 2019 to March 2020 were used to evaluate the dynamical processes driving near bed cooling at Egmont, a steep sloped atoll within the Chagos Archipelago and home to a large and highly resident reef manta ray population. The basin-scale oceanographic regime, particularly the IOD, exerted a controlling influence on the depth of the thermocline throughout the archipelago, driving a historically deep thermocline during November 2019 and precluding the observation of cooling at 60-70 m depth. A relaxing of the IOD coupled with standard seasonal evolution resulted in a shoaling of the thermocline back into the 65-75 m depth range and the emergence of the temperature signals associated with manta presence, driven at semi-diurnal frequencies.

At tidal, and subtidal frequencies differences in the thermal regime were seen between the central Manta Alley mooring and the Western Manta Alley, and Ile De Rats moorings, despite a separation distance of just 2.7 km. Simultaneous near-bed cooling was observed at tidal frequencies at both sites with time synchronicity which precludes a freely propagating along-slope internal tide as the driver. At both sites high frequency internal waves with periods, T, < 20 minutes were observed and associated with subcritical Ri values, indicating the capacity of these waves to generate mixing through shear instability that may influence zooplankton distributions and thereby manta foraging efficiency.

Some observed signals are consistent with the presence of mode-2 waves generated downstream of interaction with steep topography. However, the complex local topography makes the differentiation between mode-2 and mode-1 waves difficult. Wavelet analysis shows that the internal wave activity varies in intensity, likely governed by the prevailing stratification and shear environments, and serves as a reminder that these processes have extremely complex interactions that are challenging to resolve either with in-situ observations or though numerical modelling.

The differences in tidal and sub-tidal cooling measured along Manta Alley demonstrates that, in highly dynamical regimes, changes in the physical environment occur over short spatiotemporal scales. This fine scale variability will generate changes in the underlying ecosystems, which may then play a role in influencing the site preferentiality of highly mobile species such as reef manta rays. Overall, this demonstrates the need to understand the fine scale dynamics when working at highly energetic sites where reliance on coarse remote products, either satellite derived or modelled, produces an erroneous perspective of physical processes at these sites where high frequency energetic dynamics are underrepresented and local environmental gradients are occluded into single data points.

7 – Acknowledgement

This study was made possible by funding from the Garfield Weston Foundation, and the Bertarelli Foundation, whom we thank for their generous support in making this work possible. We also thank the numerous people who provided support in the field, including the technical and research teams at the University of Plymouth, and the vessels crew.

References

A. Cordeiro, T. *et al.* (2013) ‘Deep Chlorophyll Maximum in Western Equatorial Atlantic - How does it Interact with Islands Slopes and Seamounts?’, *Marine Science*, 3(1), pp. 30–37. Available at: https://doi.org/10.5923/j.ms.20130301.03.

Abram, N.J. *et al.* (2008) ‘Recent intensification of tropical climate variability in the Indian Ocean’, *Nature Geoscience*, 1(12), pp. 849–853. Available at: https://doi.org/10.1038/ngeo357.

Andrzejaczek, S. *et al.* (2020) ‘Individual variation in residency and regional movements of reef manta rays Mobula alfredi in a large marine protected area’, *Marine Ecology Progress Series*, 639, pp. 137–153. Available at: https://doi.org/10.3354/meps13270.

Armstrong, A.O. *et al.* (2016) ‘Prey Density Threshold and Tidal Influence on Reef Manta Ray Foraging at an Aggregation Site on the Great Barrier Reef’, *PLOS ONE*. Edited by J.-S. Hwang, 11(5), p. e0153393. Available at: https://doi.org/10.1371/journal.pone.0153393.

Armstrong, A.O. *et al.* (2019) ‘Photographic identification and citizen science combine to reveal long distance movements of individual reef manta rays Mobula alfredi along Australia’s east coast’, *Marine Biodiversity Records*, 12(1), pp. 10–15. Available at: https://doi.org/10.1186/s41200-019-0173-6.

Armstrong, A.O. *et al.* (2021) ‘Reef manta rays forage on tidally driven, high density zooplankton patches in Hanifaru Bay, Maldives’, *PeerJ*, 9, p. e11992. Available at: https://doi.org/10.7717/peerj.11992.

Baines, P.G. (1973) ‘The generation of internal tides by flat-bump topography’, *Deep-Sea Research and Oceanographic Abstracts*, 20(2), pp. 179–205. Available at: https://doi.org/10.1016/0011-7471(73)90050-8.

Balmforth, N.J. and Peacock, T. (2009) ‘Tidal conversion by supercritical topography’, *Journal of Physical Oceanography*, 39(8), pp. 1965–1974. Available at: https://doi.org/10.1175/2009JPO4057.1.

Carr, M. *et al.* (2019) ‘Shoaling mode-2 internal solitary-like waves’, *Journal of Fluid Mechanics*, 879, pp. 604–632. Available at: https://doi.org/10.1017/jfm.2019.671.

Chen, Z.-W. *et al.* (2014) ‘Density stratification influences on generation of different modes internal solitary waves’, *Journal of Geophysical Research: Oceans*, 119(10), pp. 7029–7046. Available at: https://doi.org/10.1002/2014JC010069.

Cheng, M.H. *et al.* (2017) ‘Transformation of mode-2 internal solitary wave over a pseudo slope-shelf’, *AIP Advances*, 7(9). Available at: https://doi.org/10.1063/1.5000972.

Codiga, D.L. (2011) ‘Unified Tidal Analysis and Prediction Using the UTide Matlab Functions’, (September), p. 59. Available at: https://doi.org/10.13140/RG.2.1.3761.2008.

Couturier, L.I.E. *et al.* (2011) ‘Distribution, site affinity and regional movements of the manta ray, Manta alfredi (Krefft, 1868), along the east coast of Australia’, *Marine and Freshwater Research*, 62(6), p. 628. Available at: https://doi.org/10.1071/MF10148.

Deepwell, D. *et al.* (2019) ‘Wave generation through the interaction of a mode-2 internal solitary wave and a broad, isolated ridge’, *Physical Review Fluids*, 4(9). Available at: https://doi.org/10.1103/PhysRevFluids.4.094802.

Deepwell, D. and Stastna, M. (2016) ‘Mass transport by mode-2 internal solitary-like waves’, *Physics of Fluids*, 28(5). Available at: https://doi.org/10.1063/1.4948544.

Dilmahamod, A.F., Hermes, J.C. and Reason, C.J.C. (2016) ‘Chlorophyll-a variability in the Seychelles-

Chagos Thermocline Ridge: Analysis of a coupled biophysical model', *Journal of Marine Systems*, 154, pp. 220–232. Available at: https://doi.org/10.1016/j.jmarsys.2015.10.011.

Du, Y. *et al.* (2020) 'Thermocline Warming Induced Extreme Indian Ocean Dipole in 2019', *Geophysical Research Letters*, 47(18), pp. 1–10. Available at: https://doi.org/10.1029/2020GL090079.

Durham, W.M. *et al.* (2013) 'Turbulence drives microscale patches of motile phytoplankton', *Nature Communications*, 4, pp. 4–10. Available at: https://doi.org/10.1038/ncomms3148.

Farmer, D. and Armi, L. (1999) 'The generation and trapping of solitary waves over topography', *Science*, 283(5399), pp. 188–190. Available at: https://doi.org/10.1126/science.283.5399.188.

Foreman, M.G. (1977) 'Manual for tidal heights analysis and prediction, Institute of Ocean Sciences, Sidney', *Tech. Rep. Pac. Mar. Sci.* [Preprint], (January 1977). Available at: http://champs.cecs.ucf.edu/Library/Journal_Articles/pdfs/Manual for tidal heights analysis and prediction.pdf.

Fu, K.H. *et al.* (2016) 'The Deformation of Shoaling Internal Waves Observed at the Dongsha Atoll in the Northern South China Sea', *Coastal Engineering Journal*, 58(2), pp. 1–19. Available at: https://doi.org/10.1142/S0578563416500017.

Gemmrich, J.R. and van Haren, H. (2002) 'Internal wave band eddy fluxes above a continental slope', *Journal of Marine Research*, 60(2), pp. 227–253. Available at: https://doi.org/10.1357/002224002760497471.

Harris, J.L. *et al.* (2020) 'Gone with the wind: Seasonal distribution and habitat use by the reef manta ray (Mobula alfredi) in the Maldives, implications for conservation', *Aquatic Conservation: Marine and Freshwater Ecosystems*, 30(8), pp. 1649–1664. Available at: https://doi.org/10.1002/aqc.3350.

Harris, J.L. *et al.* (2021) 'Fine-scale oceanographic drivers of reef manta ray (Mobula alfredi) visitation patterns at a feeding aggregation site', *Ecology and Evolution*, 11(9), pp. 4588–4604. Available at: https://doi.org/10.1002/ece3.7357.

Haury, L.R., Briscoe, M.G. and Orr, M.H. (1979) 'Tidally generated internal wave packets in Massachusetts Bay', *Nature*, 278(5702), pp. 312–317. Available at: https://doi.org/10.1038/278312a0.

Holloway, P.E. and Merrifield, M.A. (1999) 'Internal tide generation by seamounts, ridges, and islands', *Journal of Geophysical Research: Oceans*, 104(C11), pp. 25937–25951. Available at: https://doi.org/10.1029/1999jc900207.

Hosegood, P., Bonnin, J. and van Haren, H. (2004) 'Solibore-induced sediment resuspension in the Faeroe-Shetland channel', *Geophysical Research Letters*, 31(9), pp. 2–5. Available at: https://doi.org/10.1029/2004GL019544.

Hosegood, P. and Van Haren, H. (2004) 'Near-bed solibores over the continental slope in the Faeroe-Shetland Channel', *Deep-Sea Research Part II: Topical Studies in Oceanography*, 51(25-26 SPEC. ISS.), pp. 2943–2971. Available at: https://doi.org/10.1016/j.dsr2.2004.09.016.

Hosegood, P.J. *et al.* (2019) 'Internal lee waves and baroclinic bores over a tropical seamount shark "hot-spot"', *Progress in Oceanography*, 172(June 2018), pp. 34–50. Available at: https://doi.org/10.1016/j.pocean.2019.01.010.

Jaine, F.R.A. *et al.* (2014) 'Movements and habitat use of reef manta rays off eastern Australia: Offshore excursions, deep diving and eddy affinity revealed by satellite telemetry', *Marine Ecology Progress Series*, 510, pp. 73–86. Available at: https://doi.org/10.3354/meps10910.

Jones, A.R. *et al.* (2014) 'Fine-scale hydrodynamics influence the spatio-temporal distribution of harbour porpoises at a coastal hotspot', *Progress in Oceanography*, 128, pp. 30–48. Available at: https://doi.org/10.1016/j.pocean.2014.08.002.

Klymak, J. *et al.* (2012) 'The Direct Breaking of Internal Waves at Steep Topography', *Oceanography*, 25(2), pp. 150–159. Available at: https://doi.org/10.5670/oceanog.2012.50.

Lamb, K.G. (2004) 'Nonlinear interaction among internal wave beams generated by tidal flow over supercritical topography', *Geophysical Research Letters*, 31(9), pp. 1–4. Available at: https://doi.org/10.1029/2003GL019393.

Leichter, J.J. *et al.* (2012) 'The island-scale internal wave climate of Moorea, French Polynesia', *Journal of Geophysical Research: Oceans*, 117(6), pp. 1–16. Available at: https://doi.org/10.1029/2012JC007949.

Lennert-Cody, C.E. and Franks, P.J.S. (1999) 'Plankton patchiness in high-frequency internal waves', *Marine Ecology Progress Series*, 186, pp. 59–66. Available at: https://doi.org/10.3354/meps186059.

Lennert-Cody, C.E. and Franks, P.J.S. (2002) 'Fluorescence patches in high-frequency internal waves', *Marine Ecology Progress Series*, 235(Baines 1986), pp. 29–42. Available at: https://doi.org/10.3354/meps235029.

Liang, J. *et al.* (2018) 'Generation of mode-2 internal waves in a two-dimensional stratification by a mode-1 internal wave', *Wave Motion*, 83, pp. 227–240. Available at: https://doi.org/10.1016/j.wavemoti.2018.09.014.

Liccardo, A. *et al.* (2013) 'Response of the deep chlorophyll maximum to fluctuations in vertical mixing intensity', *Progress in Oceanography*, 109, pp. 33–46. Available at: https://doi.org/10.1016/j.pocean.2012.09.004.

Liu, H. *et al.* (2022) 'Interannual variability of the thermocline depth in the south-central Indian Ocean: Respective influences of IOD and ENSO', *International Journal of Climatology*, 42(10), pp. 5111–5120. Available at: https://doi.org/10.1002/joc.7522.

Liu, Z., Grimshaw, R. and Johnson, E. (2019) 'Generation of mode 2 internal waves by the interaction of mode 1 waves with topography', *Journal of Fluid Mechanics*, 880, pp. 799–830. Available at: https://doi.org/10.1017/jfm.2019.679.

Lu, B. and Ren, H.L. (2020) 'What Caused the Extreme Indian Ocean Dipole Event in 2019?', *Geophysical Research Letters*, 47(11), pp. 0–2. Available at: https://doi.org/10.1029/2020GL087768.

Lü, X. *et al.* (2010) 'Upwelling and surface cold patches in the Yellow Sea in summer: Effects of tidal mixing on the vertical circulation', *Continental Shelf Research*, 30(6), pp. 620–632. Available at: https://doi.org/10.1016/j.csr.2009.09.002.

Mahadevan, A. (2016) 'The Impact of Submesoscale Physics on Primary Productivity of Plankton', *Annual Review of Marine Science*, 8, pp. 161–184. Available at: https://doi.org/10.1146/annurev-marine-010814-015912.

Muchowski, J. *et al.* (2022) 'Potential and Limitations of a Commercial Broadband Echosounder for Remote Observations of Turbulent Mixing', *Journal of Atmospheric and Oceanic Technology*, pp. 1985–2003. Available at: https://doi.org/10.1175/jtech-d-21-0169.1.

Müller, P. and Liu, X. (2000) 'Scattering of internal waves at finite topography in two dimensions, Part II: Spectral calculations and boundary mixing', *Journal of Physical Oceanography*, 30(3), pp. 550–563. Available at: https://doi.org/10.1175/1520-0485(2000)030<0550:SOIWAF>2.0.CO;2.

Nikurashin, M. and Ferrari, R. (2010) 'Radiation and dissipation of internal waves generated by geostrophic motions impinging on small-scale topography: Theory', *Journal of Physical Oceanography*, 40(5), pp. 1055–1074. Available at: https://doi.org/10.1175/2009JPO4199.1.

Peel, L.R. *et al.* (2019) 'Movement and residency patterns of reefmanta rays Mobula alfredi in the Amirante Islands, Seychelles', *Marine Ecology Progress Series*, 621, pp. 169–184. Available at: https://doi.org/10.3354/meps12995.

Rayson, M.D. *et al.* (2018) 'Resolving high-frequency internal waves generated at an isolated coral atoll using an unstructured grid ocean model', *Ocean Modelling*, 122(June 2017), pp. 67–84. Available at: https://doi.org/10.1016/j.ocemod.2017.12.007.

Reid, E.C. *et al.* (2019) 'Internal waves influence the thermal and nutrient environment on a shallow coral reef', *Limnology and Oceanography*, 64(5), pp. 1949–1965. Available at: https://doi.org/10.1002/lno.11162.

Rohner, C.A. *et al.* (2013) 'Trends in sightings and environmental influences on a coastal aggregation of manta rays and whale sharks', *Marine Ecology Progress Series*, 482, pp. 153–168. Available at: https://doi.org/10.3354/meps10290.

Roquet, F. *et al.* (2015) 'Accurate polynomial expressions for the density and specific volume of seawater using the TEOS-10 standard', *Ocean Modelling*, 90, pp. 29–43. Available at: https://doi.org/10.1016/j.ocemod.2015.04.002.

Saji, N.H. *et al.* (1999) 'A dipole mode in the tropical Indian Ocean', *Nature*, 401(6751), pp. 360–363. Available at: https://doi.org/10.1038/43854.

Thorpe, S.A. and Lemmin, U. (1999) 'Internal waves and temperature fronts on slopes', *Annales Geophysicae*, 17(9), pp. 1227–1234. Available at: https://doi.org/10.1007/s00585-999-1227-6.

Velmurugan, A. (2015) 'Tropical islands', pp. 1–41. Available at: https://doi.org/10.1090/gsm/161/01.

Vlasenko, V. and Alpers, W. (2005) 'Generation of secondary internal waves by the interaction of an internal solitary wave with an underwater bank', *Journal of Geophysical Research C: Oceans*, 110(2), pp. 1–16. Available at: https://doi.org/10.1029/2004JC002467.

Weeks, S.J. *et al.* (2015) 'Unique sequence of events triggers manta ray feeding frenzy in the Southern Great Barrier Reef, Australia', *Remote Sensing*, 7(3), pp. 3138–3152. Available at: https://doi.org/10.3390/rs70303138.

Williams, G.J. *et al.* (2018) 'Biophysical drivers of coral trophic depth zonation', *Marine Biology*, 165(4). Available at: https://doi.org/10.1007/s00227-018-3314-2.

Wolanski, E. and Delesalle, B. (1995) 'Upwelling by internal waves, Tahiti, French Polynesia', *Continental Shelf Research*, 15(2–3), pp. 357–368. Available at: https://doi.org/10.1016/0278-4343(93)E0004-R.

Xue, Y., Higgins, W. and Kousky, V. (2002) 'Influences of the Madden Julian Oscillations on temperature and precipitation in North America during ENSO-neutral and weak ENSO winters', *Proc. Workshop on Prospects for Improved Forecasts of Weather and Short-Term Climate Variability on Subseasonal (2 Week to 2 Month) Time Scales*, pp. 1–4. Available at: https://www.cpc.ncep.noaa.gov/products/precip/CWlink/daily_mjo_index/CPCmjoindex.pdf.

Zhao, Z. (2018) 'The Global Mode-2 M2 Internal Tide', *Journal of Geophysical Research: Oceans*, 123(11), pp. 7725–7746. Available at: https://doi.org/10.1029/2018JC014475.